

Simulation-based Investigation of Inner Ring Creep at the Wind turbine Main Bearing

Simulativ Untersuchung des Innenringwanderns am
Hauptlager der Windenergieanlage

The present work was submitted to the Department of
Continuum Mechanics

from

Deepak Petchimuthu

Table of Contents

Acknowledgements	2
1 Introduction	5
1.1 Drivetrain architectures	5
1.2 Failures and damage in main bearings	6
1.3 Objectives and scope of thesis	9
2 Bearing Ring Creep	11
2.1 Definition	11
2.2 Mechanism of ring creep	12
2.3 Research & recent findings	14
2.4 Factors influencing ring creep	16
3 Analysis of Ring Creep.....	18
3.1 Qualitative study	19
3.1.1 Design under study & Scope of model.....	19
3.1.2 Meshing	21
3.1.3 Interference fit	22
3.1.4 Contacts	23
3.1.5 Roller and Cage modeling	26
3.1.6 Loading	27
3.1.7 Boundary conditions	28
3.2 Quantitative study	29
3.2.1 Design under study	30
3.2.2 Meshing	31
3.2.3 Contacts & Joints	32
3.2.4 Boundary conditions	32
3.2.5 Rotation of contact forces	33
4 Results and discussions.....	34
4.1 Criterion for creep	34
4.2 Qualitative results.....	37
4.2.1 Sliding distance evaluation.....	37
4.2.1 Contact status.....	40
4.2.2 Parametric study 1.....	41
4.2.3 Parametric study 2.....	42

4.2.4 Parametric study 3.....	43
4.3 Quantitative results.....	44
4.3.1 Creep plots	44
4.3.2 Load vs tangential displacement (pattern and trend).....	46
5 Conclusion and Future work	47
References	49
Appendix (A)	51
APDL script.....	51

1 Introduction

Wind turbines are a major source of renewable energy globally and play a significant role in providing clean, climate-friendly, and sustainable energy. However, the developments and upscaling in size and power of both onshore and offshore wind turbines have been challenging the existing technological capabilities and knowledge base. Moreover, manufacturing costs, repairs, maintenance costs, and operational failures are to be limited to ensure competitiveness and economic viability. The drivetrain, which is the energy converting component from the hub to the generator, has a significant influence on these factors. Some major components of the drivetrain include the gearbox, main shaft, main bearing, bedplate, and generator. Failures related to the main bearings are found to be the second most important reliability challenge after gearboxes [1] [2]. A challenge that has been addressed in recent times is the ring creep phenomenon, which can be observed at the inner ring-shaft interface of the main bearing assembly [3] [4] [5]. The aim of the master thesis is to understand this phenomenon and develop a modeling approach for the main bearing of a wind turbine drivetrain.

1.1 Drivetrain architectures

In the last few years, several types of drivetrain technologies have been realized, each with their own pros and cons. In today's market, two conventional drivetrain concepts can be distinguished: Geared drivetrains and direct drives. A direct drive system is expensive due to its large dimensions, weight, and generator designs. But with no gearbox, which has high failure rates, these types of turbines tend to be more reliable. However, the wind industry is still opting for low and medium speed geared turbines.

These drivetrains are further divided into different architectures, among which 3-point and 4-point suspension systems are the most common. In the 3-point suspension configuration, the rotor is rigidly connected to the main shaft, which is supported by a single main bearing near the rotor. The gearbox is supported by two torque arms that are connected to the bedplate elastically. These two torque arms, along with the single main bearing, provide a total of three points of support. The 4-point suspension configuration places an additional main bearing near the downwind side of the main shaft with the intent of isolating any non-torque rotor loads

upwind of the gearbox. Main-bearing configuration is a critical design choice that affects the overall wind turbine and plant cost of energy. A typical wind turbine geared drivetrain system with all the components as per different topologies is shown in Figure.

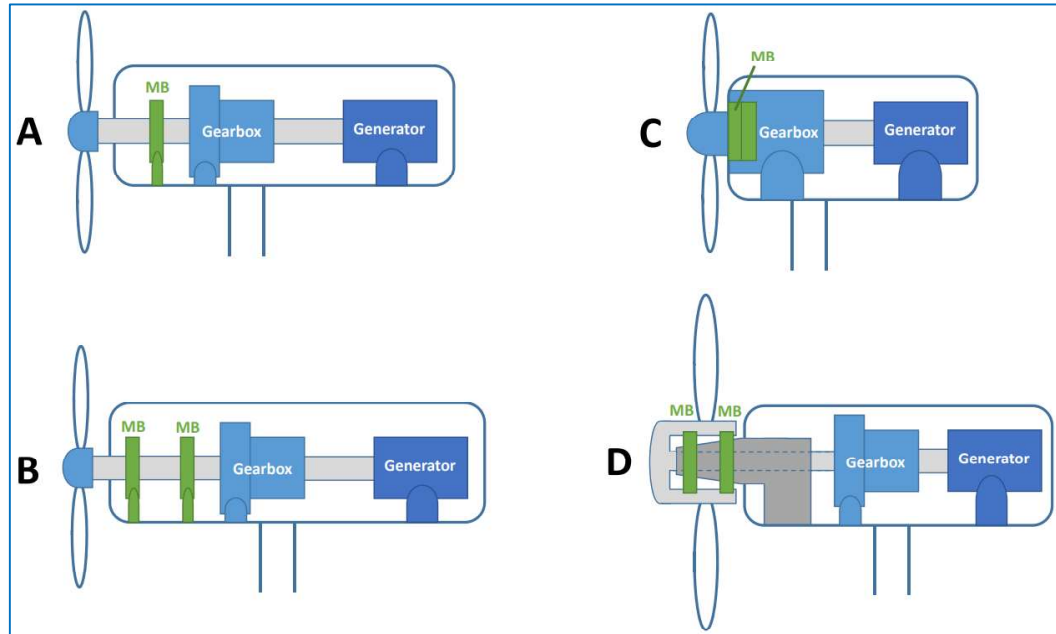


Figure 1: (A) 3-point suspension; (B) 4-point suspension; (C) Gearbox integrated; (D) Floating drivetrain [1]

The wind turbine main bearing (WTMB), depending on the type and the drivetrain configuration, transfers the majority of the non-torque loads to the bedplate. They are an integral load-carrying structure of the drivetrain, with severe cost implications in the event of failure. The typical WTMB are spherical roller bearings (SRB), cylindrical roller bearings (CRB), and tapered roller bearings (TRB). The conditions experienced by them are still not well understood and are very different than the conditions in conventional power plants [2] [1].

1.2 Failures and damage in main bearings

The conditions experienced by the WTMBs are still not well understood and are very different than the conditions in conventional power plants. It has been implied by some observations that most of the failures in main bearings under such conditions could be due to other mechanisms and not just fatigue [2]. Therefore, they don't last

up to their 20-year design life, while in some cases failing within 6 years. Moreover, the main bearing failure rates, presented as 20-year design life, were found to be up to 30% [1]. Some of the wear and damage mechanisms in WTBMs are as follows:

a. Fatigue

Dynamic contact conditions cause stress fields and plastic deformation in contacting materials, which subsequently causes fatigue cracks originating at defects or inclusions in the material structure. Such crack intersections cause pits to form and abrasive particles to be released into the bearing area. Further this will spread by itself, resulting in a rougher surface, fewer contact surfaces, and higher abrasive wear levels.

b. Micro-pitting

Micro-pitting arises from the interaction between roller and race surface asperities because of inadequate lubricant film. Such conditions are developed by high loading and off-design operation. The failure mechanism linked to surface asperity interactions often arises when there is a relative sliding between the contacting surfaces in presence of insufficient lubricant film.

c. Spalling

The pitting or flaking away of bearing material is known as spalling, and it frequently happens as a result of another major damage mechanism like micro-pitting. Spalling occurs due to geometric stress concentrations caused by misalignment, excessive loading or high localized stresses resulting from surface dents and damage or hard particle contamination.

d. Smearing

Smearing is a form of adhesive wear which occurs under sliding contact between two surfaces, involving the transfer of material from one surface to the other.

e. Abrasive wear and debris damage

Hard particles in bearing contact can lead to physical damage; either from indentations left by rolling particles, or surface scratching due to sliding particles. Similarly, particles in the lubricant, due to contamination or abrasive damage of bearing surfaces, can lead to high local stress fields and abrasive conditions. Ductile metallic debris in the lubricant can be rolled over and flattened by rolling elements, leaving larger shallow smooth dents. Brittle materials, such as sand, fractures when rolled over and leaves many small but steep sided dents. Debris damage of these types can lead to fatigue crack formation and spalling.

f. Fretting corrosion

Fretting corrosion occurs at contact interfaces where loads are transferred under oscillating relative micromovements. As a result, some material is separated from the surface and oxidized in the air. This can be avoided by giving sufficiently high joint pressure and enough lubrication.

Most of these damage mechanisms are self-perpetuating, leading to increasing amounts of similar damage. Furthermore, most of them are generated as a result of some other kind of damage. The presence of one can result in the initiation of others, for example: micro-pitting → spalling → abrasive wear [1]. Similarly, as per various investigations, it has been documented that bearing ring creep is one of the failure modes causing fretting corrosion and abrasive wear observed at bearing seats [3] [5] [1] [6] [4]. As a result, research on this phenomenon in various wind turbine bearings has gained significance recently.



Figure 2: Abrasive wear as observed at the bearing seat [5]

1.3 Objectives and scope of thesis

As discussed previously, the ring creep phenomenon has been widely associated with some damage mechanisms observed in the bearing seats of wind turbine drivelines [5] [7] [1] [4]. Extensive studies on creep have already been conducted on smaller roller bearings [6] [8] [9], and based on those findings, bearings in large wind turbines, such as main-shaft bearings, planetary gear bearings, yaw, and pitch bearings, have been the subject of ongoing research. Most of them are CRB, SRB or slewing bearings, which are highly susceptible to creep. Alternatively, modern turbines have been using TRB at the main shaft, which happen to be least prone to creep [5] [10]. But there could be certain factors that could possibly give rise to this failure mode in the future, and therefore there is a need to develop a similar modeling approach for TRB with further investigation.

The objectives of the master thesis are as follows:

- Understand the creep phenomenon as described in the literature.
- Use the modeling techniques and findings from the literature review and develop a finite element approach on par with the current state of the art.
- Get qualitative and quantitative creep results for inner ring creep.

Since the design of the TRB provided under study makes it difficult to detect ring creep, some changes have been made to the original geometry by reducing the number of rollers to trigger and visualize the qualitative components related to creep.

On the other hand, the geometry of the given tapered bearing is large for generating quantitative results. Hence, considering limited computational resources, a smaller cylindrical roller bearing has been chosen for modeling a finite element approach to specifically get quantitative results.

To summarize, a tapered roller bearing of bore size 2000 mm is analyzed qualitatively with further parametric studies, and subsequently, an approach is developed to quantitatively analyze a generic cylindrical roller bearing of bore size 100 mm, which could be replicated for the original bearing. For both cases, the inner ring creep is the subject of interest.

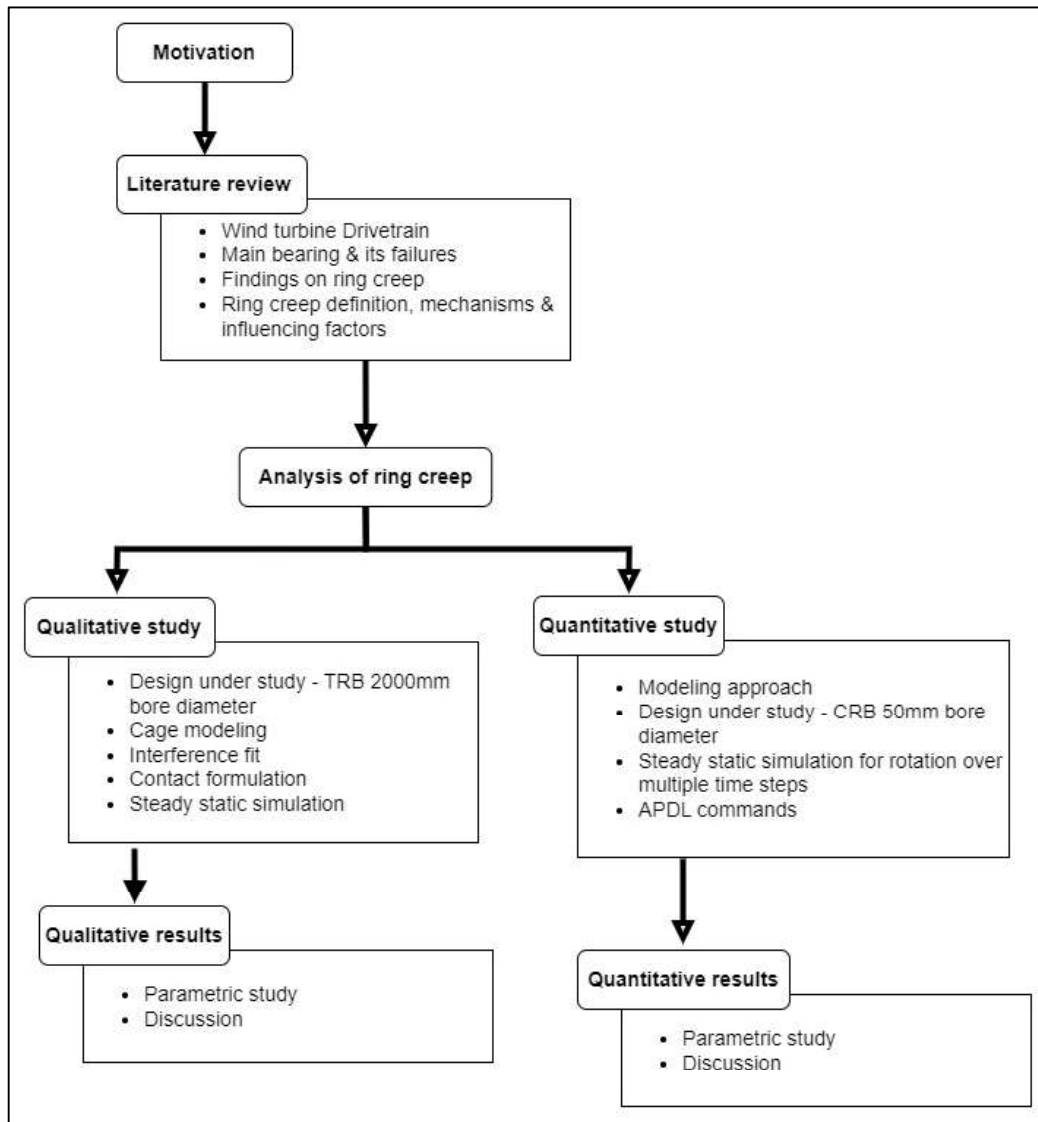


Figure 3: Thesis work flow

2 Bearing Ring Creep

2.1 Definition

Bearing ring creep is defined as irreversible micro-movements of the ring with respect to the adjacent component (housing in the case of the outer ring and shaft in the case of the inner ring). It is considered as one of the failure modes causing fretting corrosion and abrasive wear at the bearing seats, which further leads to premature failure of the bearing and high follow-up costs. It has also been detected at the respective components of the gear systems, which could further lead to meshing inaccuracies. The torque-conducting joints have been examined and modeled many times for creep, but this phenomenon in the case of support bearings is still being extensively researched.

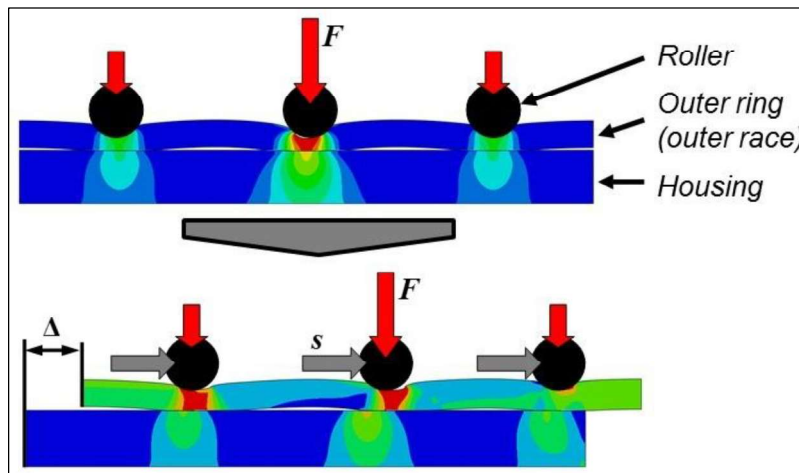


Figure 4: Simple 2D representation of creep [6]

Ring creep has been further divided into roller-induced creep and structure-induced creep. The roller-induced creep can be described as caterpillar shaped deformation due to the concentrated loading of the roller elements. This wave-like deformation further leads to a loss of contact pressure between rollers and is overcome by the tangential strain developed due to the movement of the rollers. Whereas structure-induced creep could be due to similar conditions created because of the deformation of the housing, main shaft, or gear. This type of creep is in the opposite direction to the

roller-induced creep, thereby affecting the total creep value and even reversing it in some cases.

2.2 Mechanism of ring creep

In the literature, the ring creep mechanism has been described as caterpillar-like crawling or traveling wave creeping developed due to localized strain movements. We can divide the phenomenon into two parts.

A) Static loading:

The roller element loads cause radial compression of the bearing ring at the positions directly under the rolling elements and thereby increases the local joint pressure at the interface between ring and the adjacent structure. No-slip regions are developed at such high-pressure spots. The ring material is deformed symmetrically and leads to tangential compressive stresses on the either ends of the ring-roller interface and thus, shear stress at the bearing seat.

At the same time, the bearing ring portion between the rollers bulges and causes a reduction in local joint pressure. If the local shear stresses due to roller load exceed the frictional stresses generated due to contact pressure, then a slip region is developed. These stick-slip regions generate the basis for the ring creep.

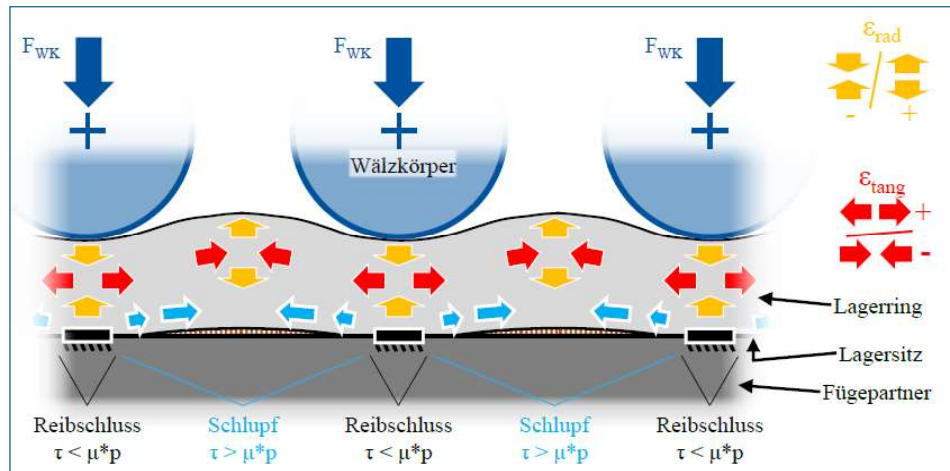


Figure 5: Static loading state [7]

B) Roller movements:

The movement of the roller elements to the right direction (as shown in Figure 6) in the loaded state leads to deformations. The material shifted to the right cannot return due to the high-pressure stick region and therefore shifts further to the right. The material rolled over on the left expands radially back to its original shape, and at the same time, shrinks tangentially. More material is added from the left side since the stick region denies the material to return back. Altogether, the entire movement of the material is in the right direction, i.e., roller movement direction. This effect occurs continuously all over the ring, and the respective displacements accumulate, leading to the global irreversible rotation of the ring with respect to the adjacent component.

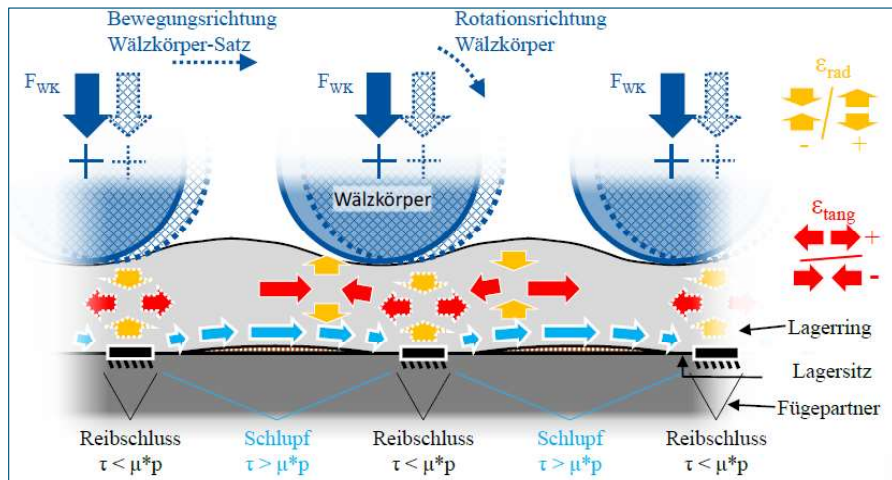
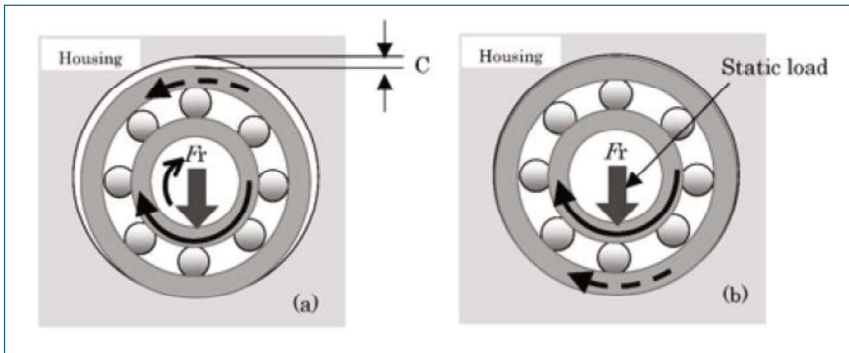
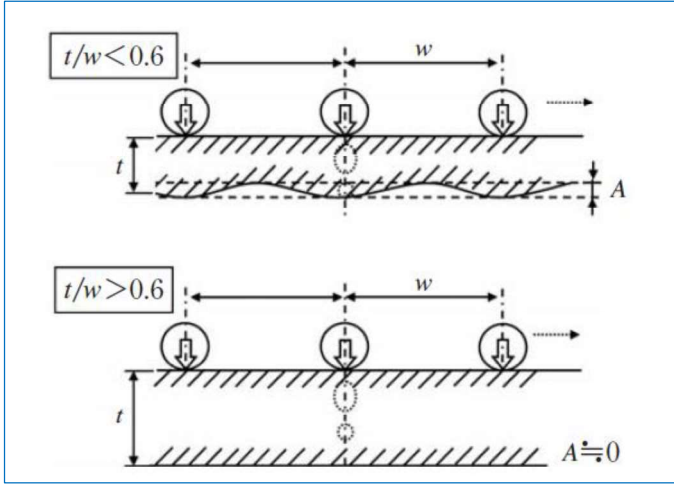


Figure 6: Rolling of loaded rollers [7]

2.3 Research & recent findings

Year	Author	Objectives & Findings
2005	Murata	<p>The research described two mechanisms of creep in terms of the type of fit between the Shaft and the Inner ring of the loaded bearing. When under interference fit, shear stresses are generated at the joint. During motion, these stresses could exceed the frictional forces which were developed due to the contact pressure and friction, leading to relative movements. Whereas under transition fit, a clearance is created due to deformation under the load which leads to geometric displacement between the inner ring and the shaft.</p> <p>The mechanism for ring creep and the condition for sliding i.e. the shear stress exceeding the frictional stress ($\tau(\theta) > \mu\sigma(\theta)$) has been introduced.</p>
2007	Zhan	<p>The study has stated mechanisms for outer ring creep and its direction depending on whether the load is rotating or static.</p> <div style="text-align: center;">  </div> <p>In the 2D FE model the housing has been kept rigid and the outer ring flexible. The rollers were replaced by point loads and distributed as per non-rotating loading.</p>

2013	Tsuyoshi NIWA	<p>The technical paper describes creep as a traveling wave and gives a criterion for the formation of wave-like deformation which is favorable for ring creep.</p>  <p>Figure 8: Wave formation criteria</p> <p>The ratio of two influencing factors, ring thickness and roller pitch should be more than 0.6 to avoid creep. The study has used Bussinesq's displacement equation.</p>
2013	Maiwald	<p>The research puts forth multiple influencing factors and a parametric study on few of them. Additionally, a calculation model was developed to get critical creeping load for outer ring under radial load. The paper also states that creep initiates when the load induced slip zone extends over entire bearing width. The model was then a part of an automated tool SimWag developed by FVA which could design creep free bearings seats.</p>
2023	Billenstein	<p>One of the most recent developments in this domain has been published by Thyssenkrupp Rothe Erde, wherein, ring creep in large bearings used in wind turbines has been investigated using simulations and experiments both. The modeling approach involves a proprietary script which applies load distribution from the contact forces instead of actual roller elements. This highly simplifies the model and gives quantitative creep results with acceptable accuracy</p>

		as verified experimentally. Moreover, the influence of friction has also been investigated in this study.
--	--	---

2.4 Factors influencing ring creep

There have been multiple influencing factors investigated that could affect ring creep in a bearing. This has led to the development of some countermeasures in the design of the bearing. Some of the important factors have been discussed below.

The coefficient of friction between the shaft and inner ring or the housing and outer ring affects creep. High friction is always beneficial for an interference fit. It could compensate for low contact pressure and avoid creep.

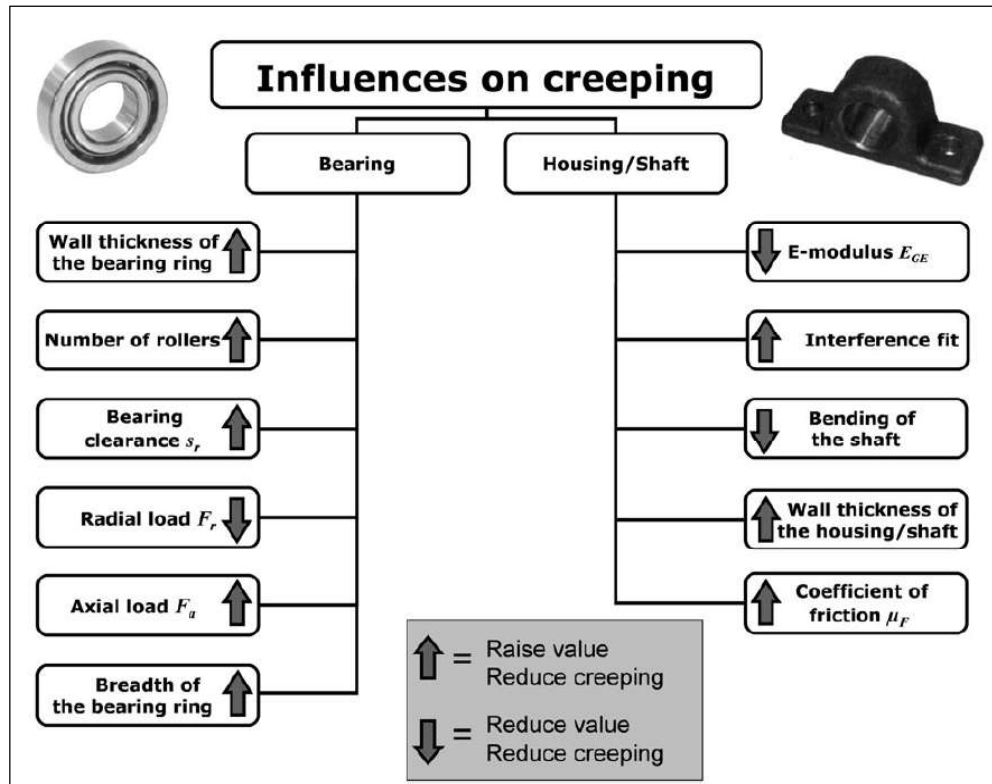


Figure 9: Influencing factors for creep [6] [10]

Interference fit at the inner ring and shaft joint, or a transition fit at the outer ring and housing joint, both have a significant impact on the creep tendency.

If sufficient oversize is not present, then the chances of creep increase. The ring thickness and the roller element pitch also have a major influence on creep, as discussed in section 2.1, and a relationship between them has already been introduced. The stiffness of the ring and adjacent components could affect the wave like formation, which is necessary for creeping. If the stiffness of the ring is low or the stiffness of the shaft or housing is high, the possibility of creep eventually increases. Also, the type of shaft (hollow or solid) and the housing stiffness distribution could affect creep.

Few types of bearings have been investigated so far, and the tapered roller bearing is found to be least prone to creep as compared to spherical roller bearings and cylindrical roller bearings [10]. The type of loading has effects on both the inner ring and outer ring creep. The shaft torsion will not be considered, assuming that the bearing doesn't carry any torsional loads. The roller effects majorly contribute to roller-induced creep, while structural effects such as shaft bending, external forces on gear teeth, and varying stiffness of housing contribute to structurally induced creep. Both creep types are opposite in direction. It has also been studied that the bending of the shaft supported as a cantilever at one end shows the best combination of both creep types [11].

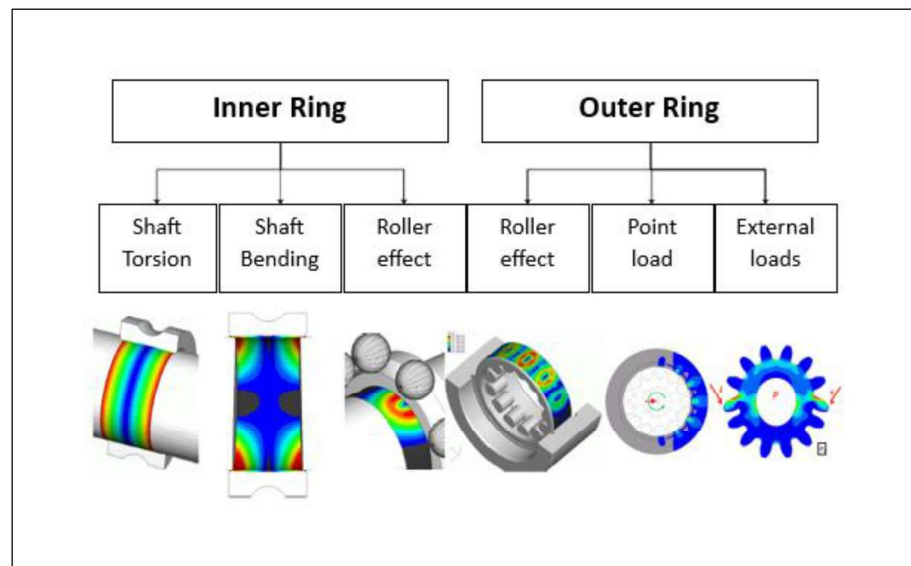


Figure 10: Loading types [11]

3 Analysis of Ring Creep

The ring creep phenomenon can be analyzed qualitatively, wherein we can only study the tendency and severity of creep. The pressure plot, status of contact, and sliding distance can be used as indicators, providing the possibility of creep. We shall use sliding distance for a parametric study based on a few of the influencing factors and verify the same with the literature. The bearing used in this case is a tapered roller bearing in the 4-point suspension drivetrain of a wind turbine.

On the other hand, quantitative results are expected in order to predict exact creep values in the bearing ring. Such simulations, including rotation of the bearing, could be expensive and time consuming because of contacts and non-linearities. To simplify the model, the roller elements are replaced by their respective contact forces and rotated using multiple time steps in the static simulation itself. This is possible using APDL commands and some preprocessing. The purpose of this part of the study is only to demonstrate the modeling approach, and therefore a smaller generic cylindrical roller bearing is used under highly simplified conditions.

In the following sub-sections, the FE-modeling approach for both cases is described. The software used for solving, pre-processing, and post-processing the model is ANSYS 2023R1.

3.1 Qualitative study

3.1.1 Design under study & Scope of model

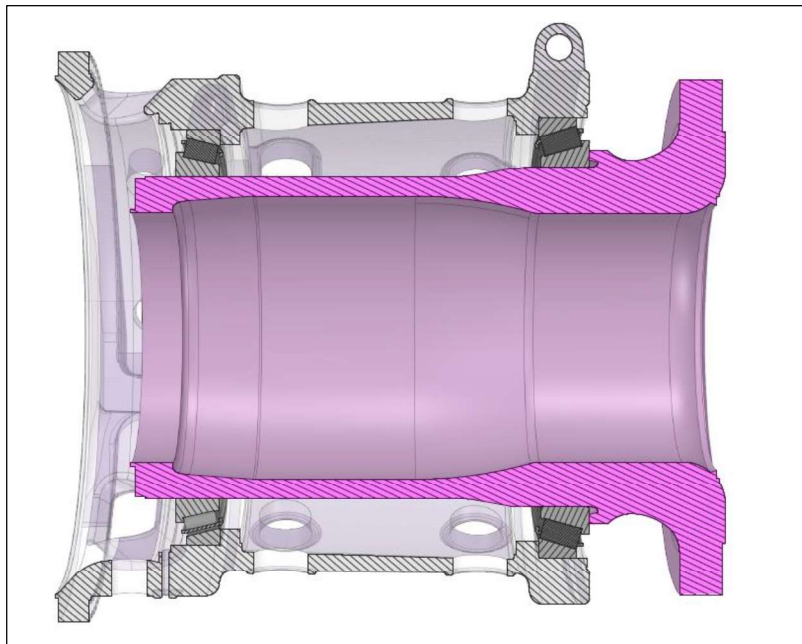


Figure 11: Drivetrain adjusted bearing arrangement

The drivetrain in the illustration is a adjusted bearing arrangement with a hollow shaft supported by two main bearings in "O" configuration. These are tapered roller bearings having 54 roller elements without any crowning. Both the bearings in this type of configuration take high amounts of axial loading. Since the bearing to the hub side is of interest in this study of creep, the other bearing towards the generator side is replaced by a normal support. Furthermore, as ring creep is to be examined at the interface between the inner ring and main shaft, the housing is neglected. By eliminating some of its geometric features that are not significant, the main shaft is further simplified.

The material defined for all the components is Structural Steel with Young's modulus 200 GPa and Poisson's ratio 0.3.

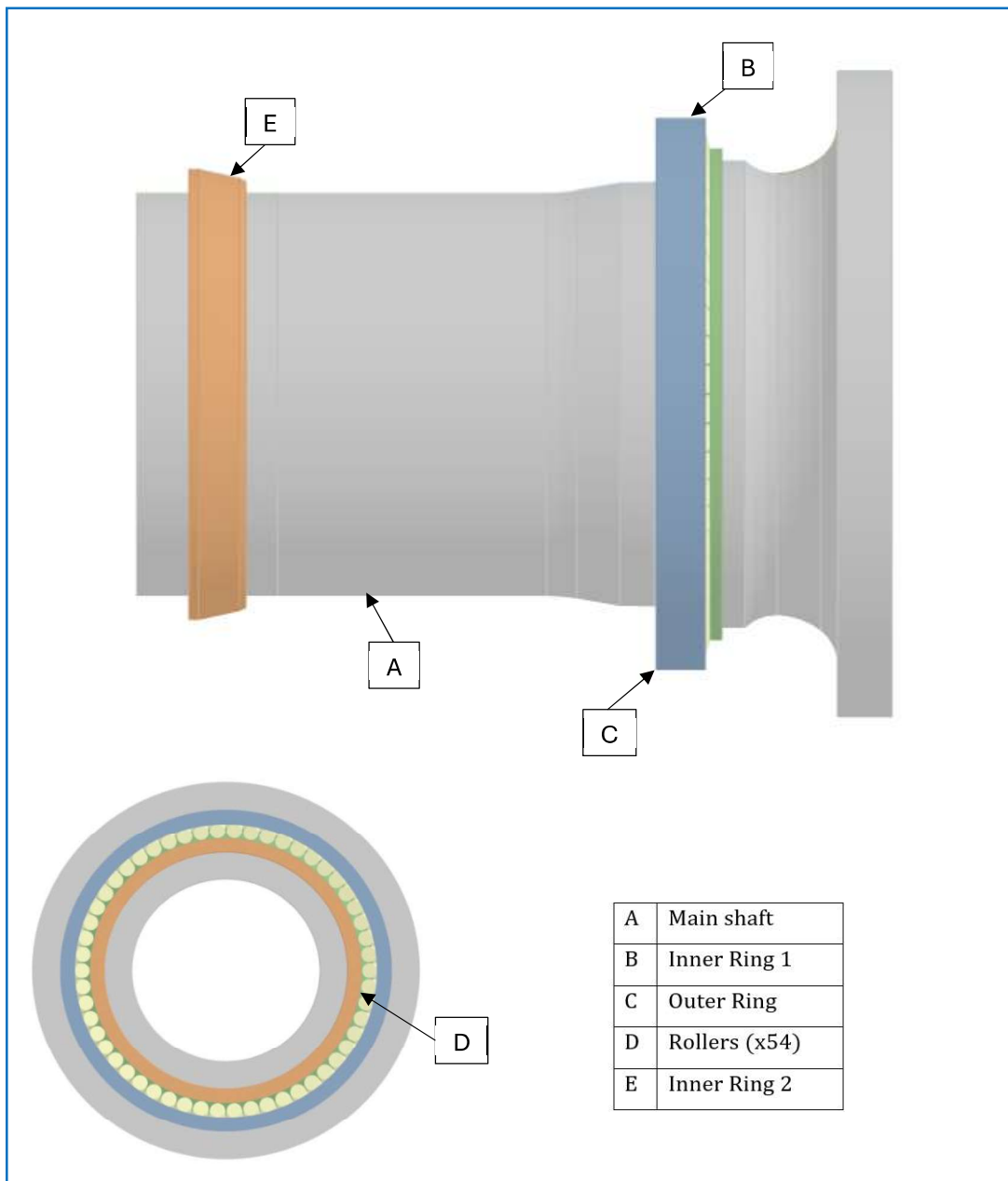


Figure 12: Geometry to be modeled for creep

3.1.2 Meshing

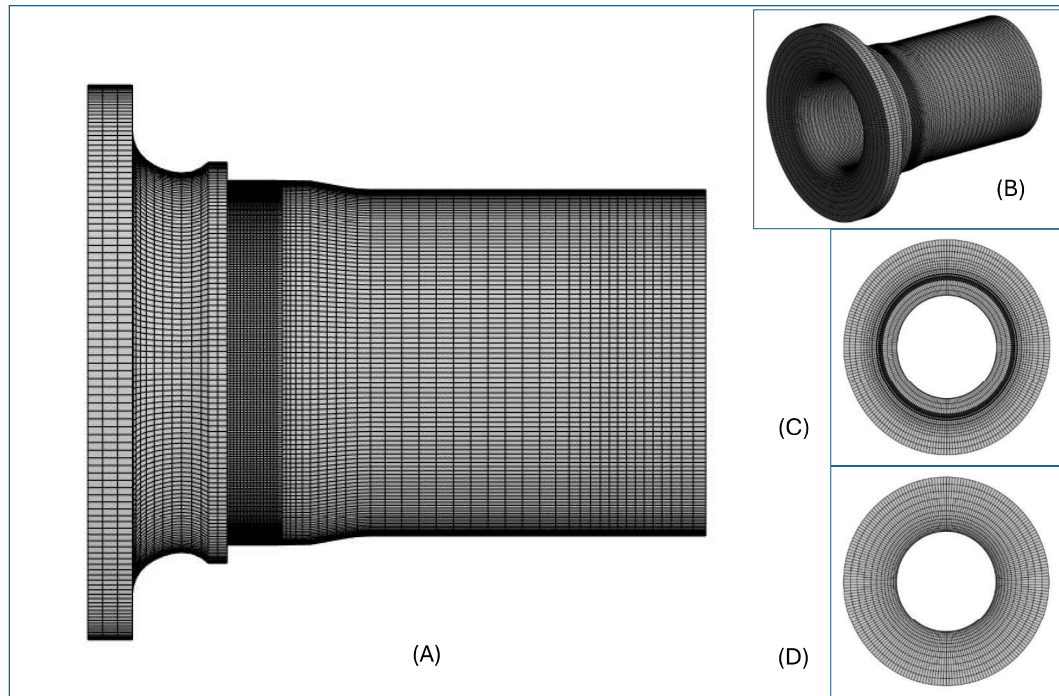


Figure 13: Meshed main shaft; Views: Side (A), Isometric (B), Front (C), Back (D)

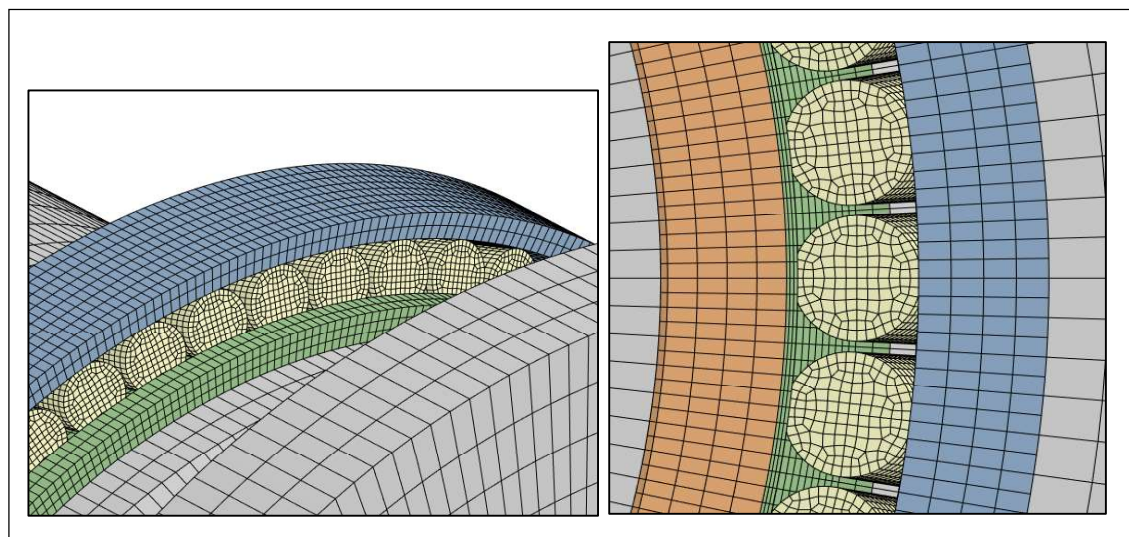


Figure 14: Complete meshed geometry

The entire model is flexible and is meshed majorly using SOLID185 elements. In the previous research linear elements have been preferred instead of higher order elements, citing convergence issues [11] [10]. In this study as well, linear elements have exhibited better convergence while higher order elements failed to converge due to element distortion. Therefore, linear elements have been chosen for the main shaft and the rings. While quadratic elements have been chosen for rollers. Moreover, the elements are well structured for the rings and shaft, and symmetrical for rollers. Between each roller pair, equal number of nodes are present and are structured to be radially in-line as shown in the Figure 14. This will ensure consistency in the results and avoid any variations due to the mesh.

	Components	Elements	Nodes
A	Main Shaft	112320	139100
B	Inner Ring 1	36288	46224
C	Outer Ring	12528	18144
D	Roller elements (per roller)	1920	2384
E	Inner Ring 2	13824	19008

Table 1: Mesh count

3.1.3 Interference fit

The fit between the inner ring and the main shaft is created by an appropriate interference during assembly. The interference fit can be easily modeled in Ansys by two methods [12]. A CAD model with an existing overlap in the components can be directly modeled. The other way is to import the CAD model with geometries having nominal diameters. In this approach an offset value can be set while defining the contact. A positive value will ensure interference, while a negative value will introduce a clearance. In addition, the ramped effects option can be chosen to ensure better convergence. If the diametrical overfit is given as 0.04 mm, then the offset must be set as half of that value, which would be 0.02 mm. With proper overfit value, the interference fit will be resolved in the first load step. Moreover, the friction needs to be turned off while solving the fit to ensure there are no additional shear stresses introduced in the model. This is possible using

APDL commands inserted in the frictional contact object in the tree. While the friction is off, additional boundary conditions are used to avoid any rigid body motion.

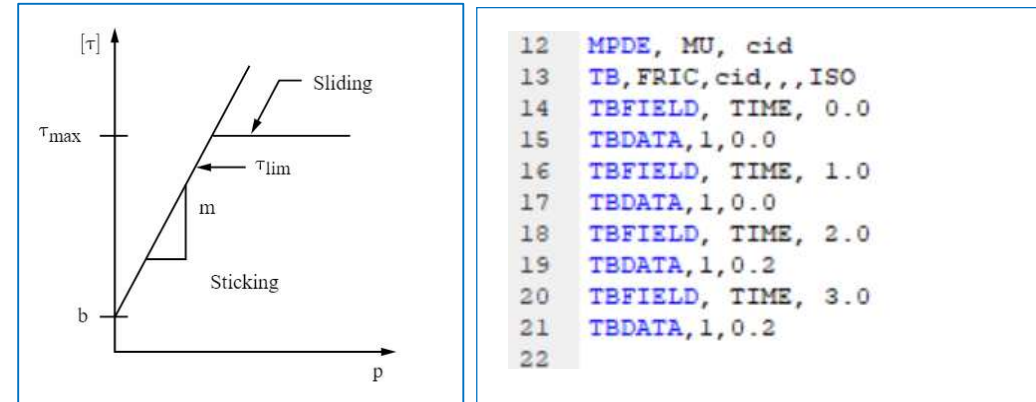


Figure 15: Coulomb friction model [12]

Figure 16: APDL command to activate friction

3.1.4 Contacts

The contact between the inner ring and shaft of the bearing under study is defined as frictional with the value of coefficient of friction as 0.2. This contact is of the highest importance and must be defined carefully. Ansys by-default utilizes a simple model of Coulomb's friction law [12]. It defines the condition which allows two surfaces to stick or slide when in contact.

$$\text{Coulomb's law:} \quad \tau_{lim} = \mu P + b$$

$$||\tau|| \leq \tau_{lim}$$

Where,

τ_{lim} = limiting frictional stress

$||\tau||$ = equivalent shear stress at the surface

μ = coefficient of friction

P = contact normal pressure

b = contact cohesion

Both the surfaces in contact carry shear stresses. When these shear stresses exceed the limiting frictional stress, the surfaces start to slide relative to each other.

While defining the contact, the values of normal stiffness and tangential stiffness, both could affect the creep and relevant quantities significantly. Normal stiffness is required to define the penetration and normal displacement between the contact pairs. Ideally it should be set to a minimum value to avoid the chattering effect. While the tangential stiffness controls the elastic slip or the relative sliding between the contact pairs. Both these values are to be set appropriately to get better convergence, but at the expense of accuracy.

Since ring creep is a critical phenomenon and demands best accuracy, the contact type of Normal Lagrange has been chosen instead of Augmented Lagrange. This will eliminate the need to define normal stiffness. Unfortunately, the tangential stiffness cannot be defined for this contact type but can be controlled using Elastic slip tolerance. The contact status will remain 'Sticking' until the value of elastic limit is reached. This value can only be determined experimentally or from literature.

Details of "Frictional - Pull (Revolve) 2(Shaft) To Pull (Revolve):Body_2(Ring)	
Contact Bodies	Pull (Revolve) 2(Shaft)
Target Bodies	Pull (Revolve):Body_2(Rings)
Protected	No
Definition	
Type	Frictional
Friction Coefficient	0,
Scope Mode	Automatic
Behavior	Program Controlled
Trim Contact	Off
Suppressed	No
Display	
Element Normals	No
Advanced	
Formulation	Normal Lagrange
Small Sliding	On
Detection Method	Nodal-Dual Shape Function Projection
Elastic Slip Tolerance	Value
Elastic Slip Tolerance Value	4,e-003 mm
Stabilization Damping Factor	0,
Pinball Region	Radius
Pinball Radius	5, mm
Time Step Controls	None
Geometric Modification	
Interface Treatment	Add Offset, Ramped Effects
Offset	0,3 mm

Figure 17: Contact settings for inner ring - shaft

Hence, the value chosen in this study is estimated in accordance with previous research [11] on this phenomenon and considering the differences in bearing sizes. The tolerance value set is 0.004 mm. A parametric study has been conducted to exhibit its significance in calculating creep and its need of further investigations. Additionally, the option of small sliding can be activated to improve convergence and efficiency. This option is used if the relative sliding between the contacts is very small as compared to the element edge length.

Details of "Frictionless - Component1\GP302993_2(Rollers-28) T▼"	
Contact Bodies	Component1\GP302993_2(Rollers-28)
Target Bodies	Pull (Revolve):Body_2(Rings)
Protected	No
Definition	
Type	Frictionless
Scope Mode	Manual
Behavior	Asymmetric
Trim Contact	Off
Suppressed	No
Display	
Element Normals	No
Advanced	
Formulation	Augmented Lagrange
Small Sliding	Off
Detection Method	Nodal-Projected Normal From Contact
Penetration Tolerance	Program Controlled
Normal Stiffness	Program Controlled
Update Stiffness	Each Iteration
Stabilization Damping Factor	0,
Pinball Region	Program Controlled
Time Step Controls	None
Geometric Modification	
Interface Treatment	Add Offset, Ramped Effects
Offset	0, mm

Figure 18: Contact settings for roller - inner ring

The contacts between the roller elements and inner ring are defined as frictionless. The formulation can be chosen as Augmented Lagrange in this case. Moreover, nodal type of detection is used as it is prescribed for contacts having edge nodes. The geometry has defined clearances at the roller and ring surface; therefore, the offset is set to 0. This quantity can be set to a negative value to give a clearance while modeling. Also, the contacts between the roller elements and the outer ring are defined bonded to further simplify the model, since we are just investigating inner ring creep.

3.1.5 Roller and Cage modeling

The creep phenomenon as studied previously is purely due to movement of the contact forces and therefore rolling can be neglected by keeping the contact frictionless without rotation of the rollers about their own axis.

To keep the model simple, the cage need not be physically present in the geometry. Hence, the way rollers and cage are modeled does play an important role because it defines how the rollers are constrained while avoiding any rigid body motion in absence of the cage. In the literature, the rollers have been individually linked using prismatic joints to a pilot node at the center. Prismatic joints are single DOF kinematic pairs which only allows sliding motion between two bodies without any rotation. This allows the rollers to move only radially as shown in the illustration below. The dotted diagram refers to a deformed state with red lines as a path followed by the roller elements.

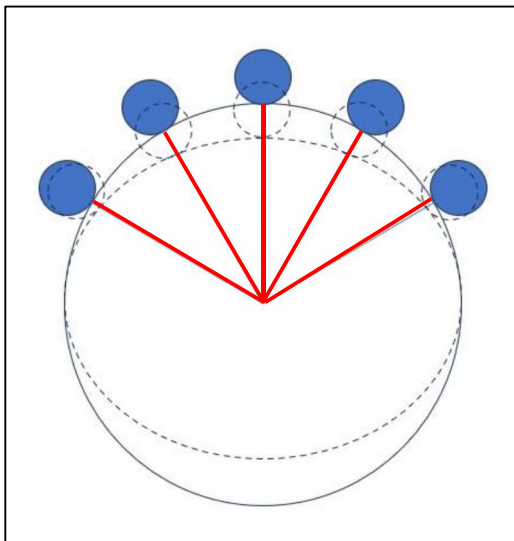


Figure 19: Roller movement along a line

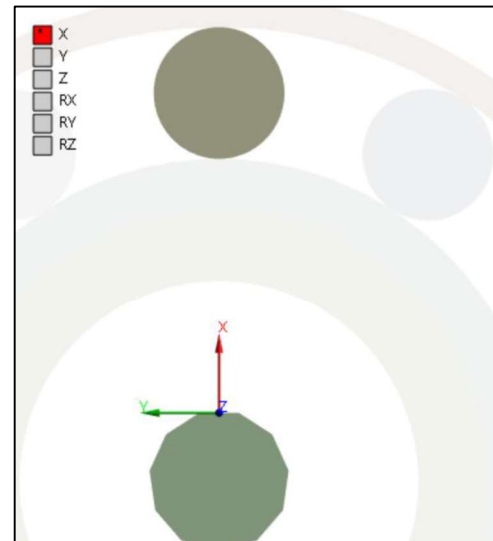


Figure 20: Translational joint for 1 roller

This modeling approach constrains the rollers perfectly for cylindrical roller bearings without the need of a cage and avoiding rigid body motion at the same time. This can be achieved by using translational joints in Ansys. One can include an additional rigid body of a polygonal prism shape for defining references for each roller joint. But in case of tapered roller bearings, we have a contact angle due to which the roller elements may not follow the same way of deformation and could

be over-constrained if the previous technique is used . As a workaround in this study, a general joint has been defined with 2 translational DOFs and one of the rotational DOFs set free as shown in the figure. This will ensure radial and axial motion of each roller without over-constraining.

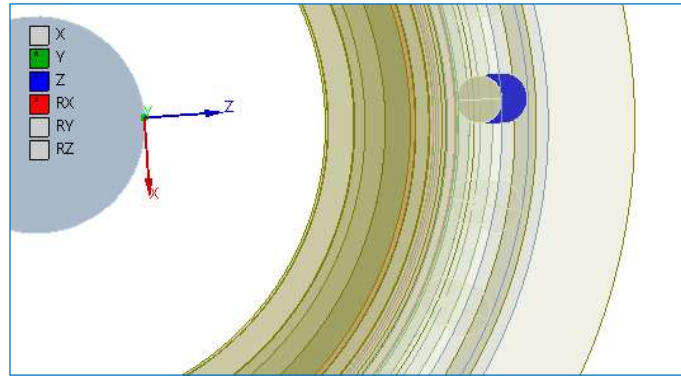


Figure 21: General contact for a roller in TRB

3.1.6 Loading

The loading of the model can be divided into 3 load steps or more, depending on the type of external loads.

Load step 1:

A friction free contact is created at the Shaft - Inner ring joint. The Contact type is used as frictional with coefficient of friction value as zero. This is necessary to avoid any kind of additional shear stresses. Moreover, additional boundary conditions are applied to prevent any rigid body motion, which are removed in the later load steps.

Load step 2:

Friction is activated in this load step as described in section 3.1.3. This step has no real loading. Also, the additional boundary conditions are removed.

Load step 3:

A force load is applied as a Remote Force at the hub end of the shaft. This type of loading will cause bending of the shaft, under which creep will be studied.

3.1.7 Boundary conditions

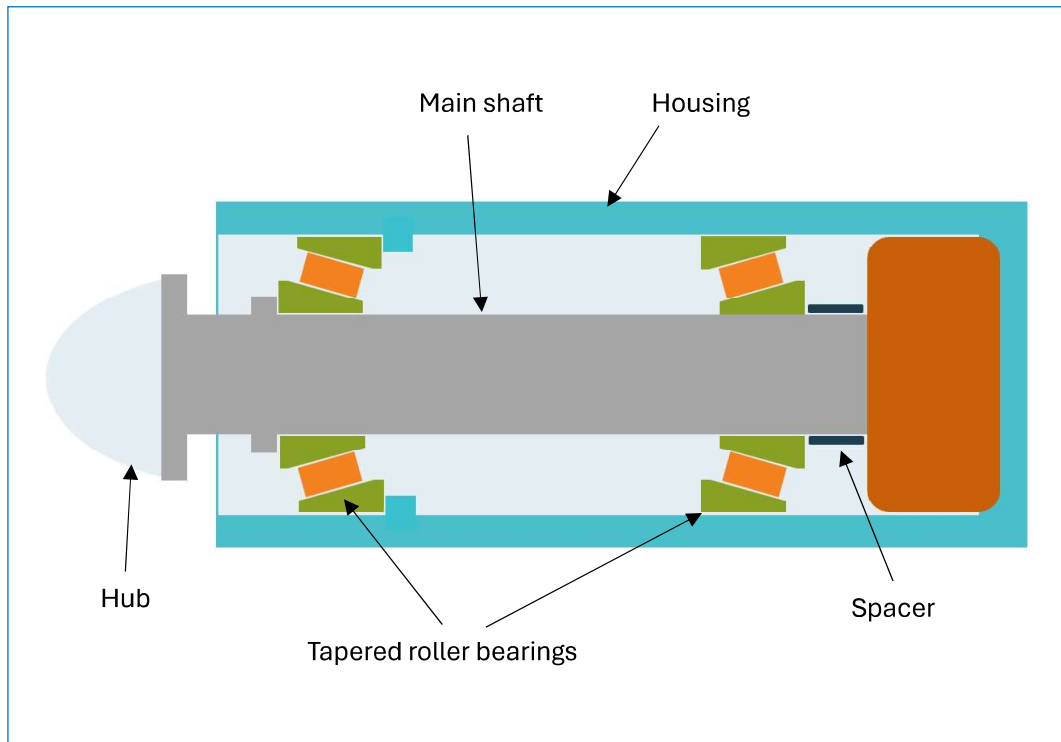


Figure 22: Graphic representation of original geometry

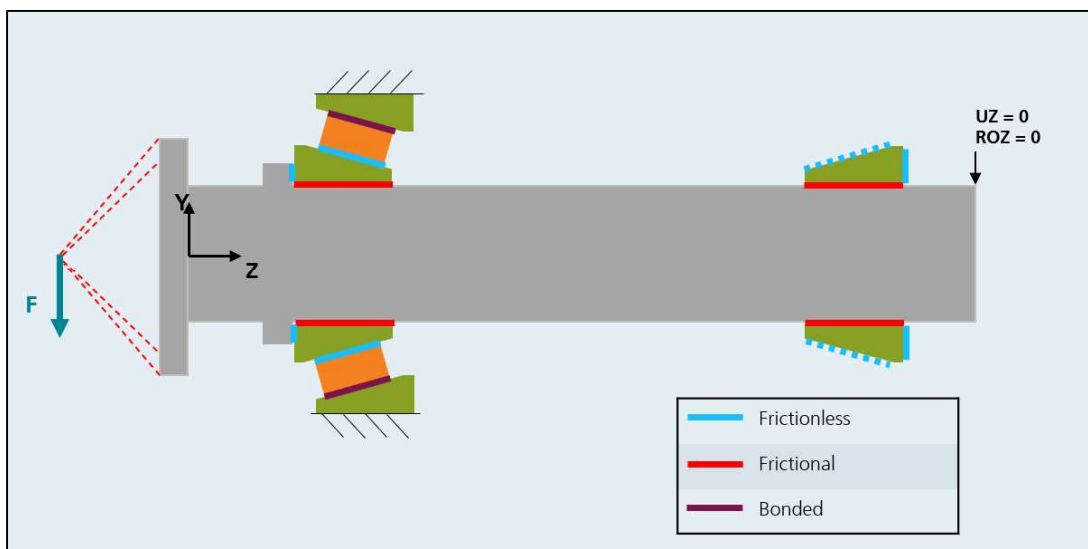


Figure 23: Model scope, Boundary conditions and contacts

The original geometry has been illustrated in Figure 23 with all the components. It is simplified as explained in section 3.1.1 and the same is described in Figure 24. The outer ring is fixed and its contact with the roller elements is bonded, since creep in the inner ring is the focus of this study.

The inner ring has contacts as defined earlier and is given additional boundary condition of remote displacement with rotational DOF fixed along the axis to prevent rigid body motion during the first load step. This condition is removed in the second load step. The second inner ring towards the generator side is just included to provide support and plays no major role in the study. Its contact with the main shaft is similar to the contact of the inner ring at the hub side. Moreover, the outer surface of the ring is given the compression only support which is equivalent to a rigid-flexible frictionless contact. One of its sides is supported by a spacer and could be given as frictionless support instead.

The shaft end towards generator is given a remote displacement with only axial displacement and rotation about the axis as fixed. The rigid cage which guides all the roller elements is given a remote displacement with all the DOFs fixed.

Lastly, a deformable remote force of 10MN is given at the distance of 1000 mm from the flange. The model solved as per the given boundary conditions and contact definitions and further parametric studies on the interference fit, coefficient of friction and load magnitude is performed.

3.2 Quantitative study

This study involves APDL scripting for applying forces. The model is divided into two parts. The first part is steady static with all the geometry without any simplification. The contact forces are calculated and exported for further processing. In the second part the model is reduced to just the shaft and inner ring with only one contact. This simplifies the model significantly by reducing the number of elements and contacts. The contact forces are then applied to the outer surface of the inner ring of the simplified model and rotated using APDL commands.

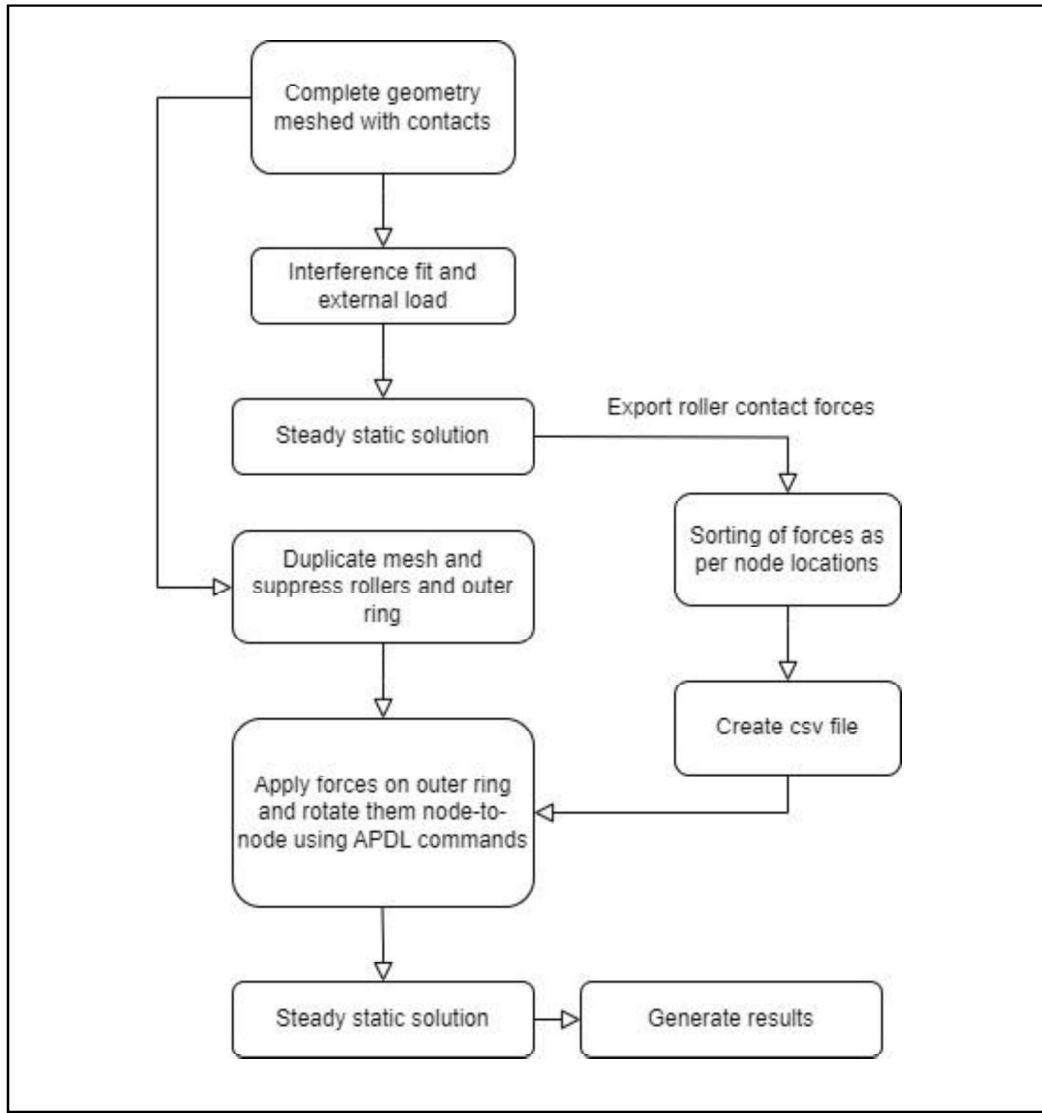


Figure 24: Modeling approach for quantitative study

3.2.1 Design under study

A cylindrical roller bearing of bore diameter 100 mm with 11 rollers is considered for this part of study. It is a simple model comprising of a hollow main shaft, inner ring, outer ring and rollers. All the bodies are flexible, except for the rollers and the cage which is just used for guiding the rollers.

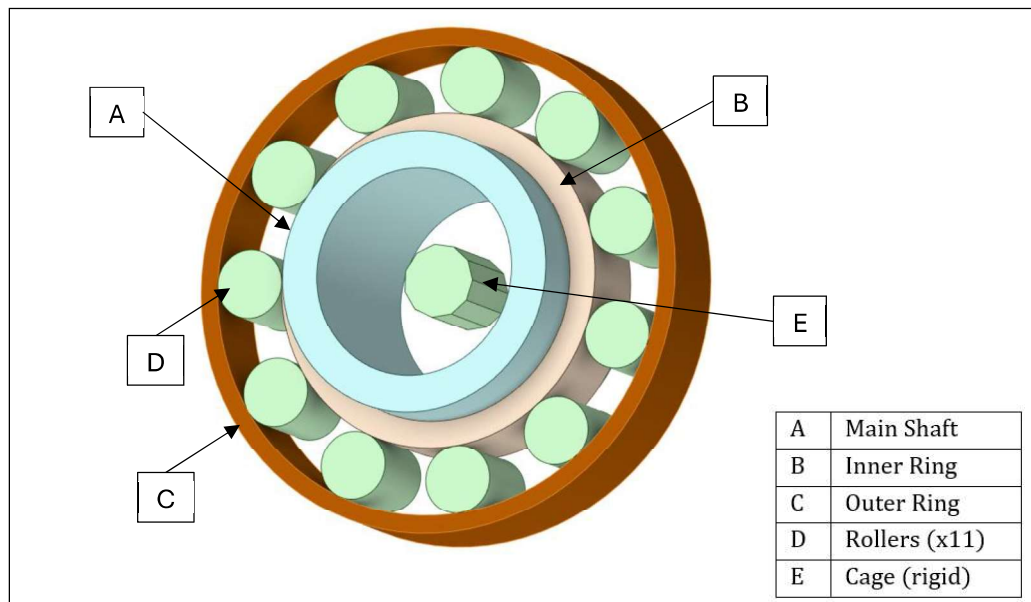


Figure 25: Geometry of a CRB under study

3.2.2 Meshing

The entire model is meshed using SOLID185 linear elements, structured equally between each roller. The contact elements CONTA173 and TARGE170 are present at the respective contact surfaces.

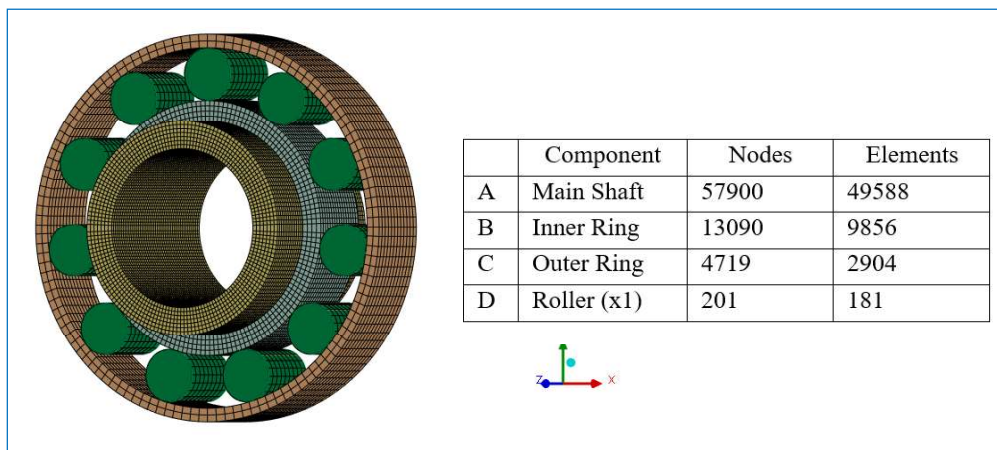


Figure 26: Meshed geometry

3.2.3 Contacts & Joints

The contacts and joints defined are similar to the ones defined in the qualitative study part. A frictional contact is defined at the main shaft and inner ring joint with an interference fit of 0.04 mm by using an offset of 0.02 mm. The coefficient of friction is set to 0.1 and elastic slip tolerance as 0.0001 mm. Whereas frictionless contacts are defined between rollers and inner ring, and bonded contacts between rollers and outer ring. The rollers and cage are modeled with translational joints as described in section 3.1.5 for cylindrical roller bearings.

3.2.4 Boundary conditions

The boundary conditions in this study are different and simpler. The shaft is not under bending load, instead it is fixed. The forces are applied to a part of the outer ring to allow only a few rollers to come under the effect. This kind of loading is being applied to create roller effects at the contact surface. An additional remote displacement is also applied to the inner ring to avoid rigid body motions in the first step. This is later removed once friction comes into action. The discussed boundary conditions are included for the first step of steady static solution. Later when the outer ring and rollers are removed and replaced by roller contact forces, only the boundary conditions for the shaft and inner ring remain.

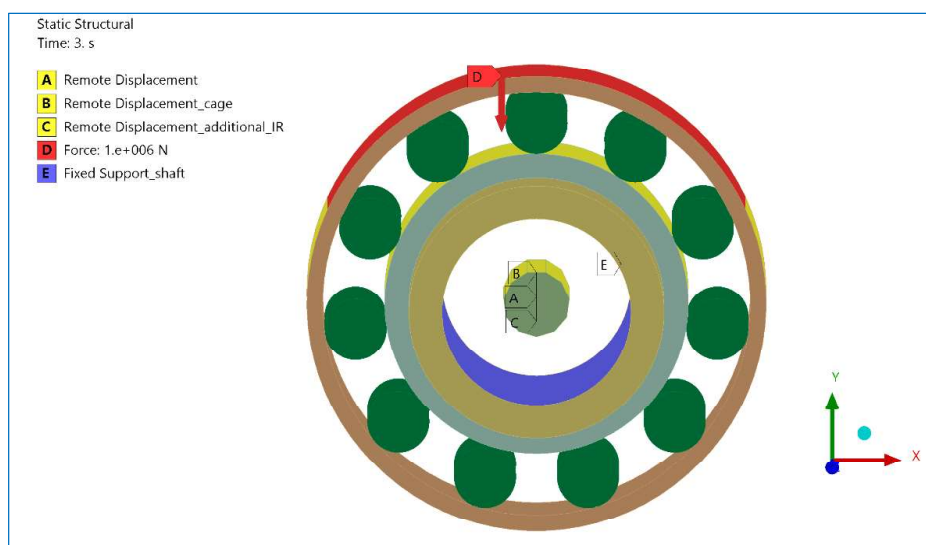


Figure 27: Boundary conditions as applied in ansys

3.2.5 Rotation of contact forces

The forces along with the nodal information are exported in xls format. It consists of the node numbers, corresponding nodal coordinates in cartesian system and the forces in all 3 directions.

The contact forces exported from the previous step are processed further. The nodes and their corresponding forces are ordered in a specific way, such that the nodes along the width of the ring are together so that the forces can be shifted along the circumference node by node. This will replicate the motion of the rollers around the inner ring.

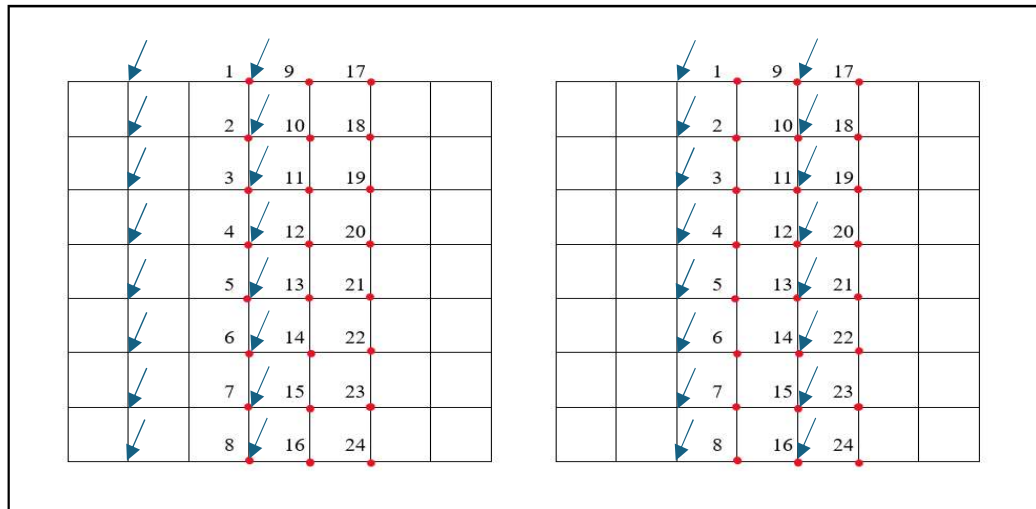


Figure 28: Forces shifting node by node along the ring circumference

For example, consider the mesh in Figure 29 horizontally along the circumference and vertically along the width of the ring. The mesh nodes are arranged in the table while fulfilling the numbering as shown. The forces in one of the load steps at the position of nodes 1-8 in Figure 29 (left) will be shifted by an offset of 8 in the next load step to the nodes 9-16. This will be done for all the forces along all the node sets in multiple load steps. The APDL script required to rotate forces is inserted along with the other boundary conditions.

4 Results and discussions

4.1 Criterion for creep

For creep to initiate certain criteria need to be fulfilled. The sliding condition between two rollers should cover the complete or most of the width of the bearing ring for creep to initiate [10]. This depends on the influencing factors which could generate wave-like deformation along the width [10]. As mentioned in the objective, some changes were made in the geometry to get the conditions favorable for ring creep. Looking at the criteria described in the findings of one of the technical papers, the thickness(t) of the ring and the roller pitch(w) are essential in creating the favorable conditions of wave-like deformation [8].

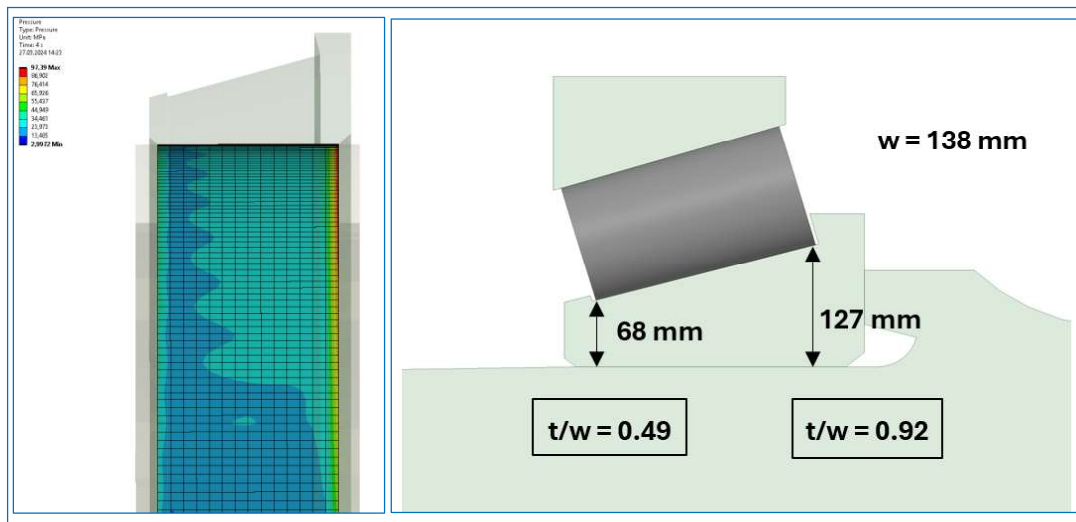


Figure 29: Contact pressure with all rollers (left); creep criteria (right)

But in case of the tapered roller bearing, the thickness varies and therefore only some part of inner ring fulfils the criteria of being less than 0.6. This can be visualized in the pressure plot, where waves stop forming due to high thickness and the rollers being too close to each other. Hence, the number of rollers is to be halved so that the ratio goes below 0.6 .

Ansys provides us with the possibility to calculate sliding distance, pressure, frictional stress, nodal forces and contact pressure, all of which have a direct relation

with the ring creep and can be used as indicators. Therefore, some of these quantities will be used for qualitative assessment of creep phenomenon in this study.

The sliding distance gives the total relative movements between a contact pair and can be calculated in the contact tool provided in ansys. There are different quantities for sliding distance depending on the direction and the way values are calculated. Since we are interested in tangential sliding along the circumference as an algebraic sum, we shall consider one of the relevant quantities.

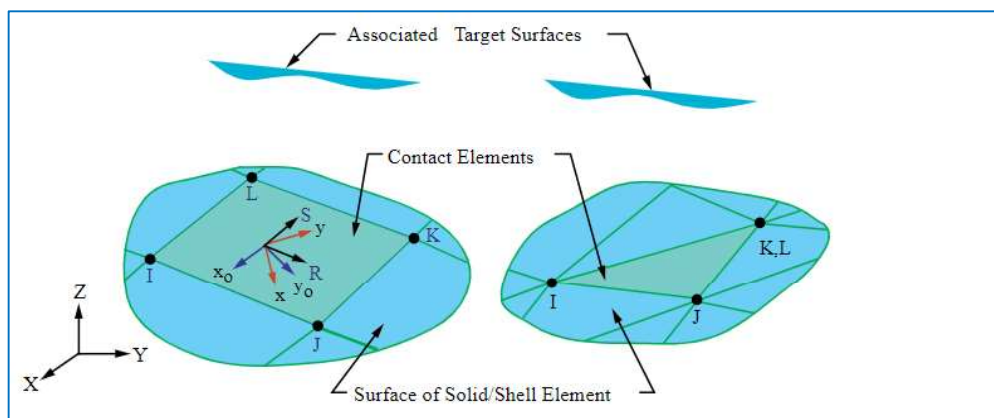


Figure 30: 4-node contact element CONTA173 [13]

The contact pair type generated for linear solid elements are CONTA173 and TARGE170 contact elements with four nodes and the orientation as described in the figure. The contact normal points towards the target element and the node ordering are as per right-hand rule. The coordinates R and S are defined for the contact element.

Quantity Name	Definition	ETABLE and ESOL Command Input					
		Item	E	I	J	K	L
PRES	Contact Pressure	SMISC	13	1	2	3	4
TAUR	Tangential contact stresses	SMISC	-	5	6	7	8
TAUS	Tangential contact stresses	SMISC	-	9	10	11	12
TASR	Total (algebraic sum) sliding in R direction	NMISC	-	17	18	19	20
TASS	Total (algebraic sum) sliding in S direction	NMISC	-	21	22	23	24
AASR	Total (absolute sum) sliding in R direction	NMISC	-	50	51	52	53
AASS	Total (absolute sum) sliding in S direction	NMISC	-	54	55	56	57
SLTO	Allowable elastic slip	NMISC	-	120	121	122	123
ELSI	Total equivalent elastic slip distance	NMISC	-	136	137	138	139
VREL	Equivalent sliding velocity (slip rate)	NMISC	-	156	157	158	159
PLSI	Total (accumulated) equivalent plastic slip due to frictional sliding	NMISC	-	164	165	166	167
GSLID	Amplitude of total accumulated sliding (including near-field)	NMISC	-	168	169	170	171

Table 2: ETABLE and ESOL command input [13]

The sliding distance in the contact tool is calculated by the quantity CONTSLID and is defined as $\sqrt{TASR^2 + TASS^2}$. It is an amplitude of accumulated sliding distances at the end of a load step from the starting position and will always be positive. Also, the sliding distance values generated at the end of second load step are to be subtracted from the values of final load step to eliminate the unnecessary sliding occurred during interference fit. Therefore, directly using CONSLID values could be misleading and there's a need for more post-processing.

The individual quantities TASR and TASS which are algebraic sum of sliding distances in R and S direction respectively will be calculated separately at the end of second and third load step. For better accuracy all the components (I,J,K and L) of a quantity can be averaged, but only one of the components(i.e. only I) will be used for evaluation. As per the table, the respective components for node I, which are CONTNMISC17 and CONTNMISC21 are calculated at the end of second and third load step. These are individually subtracted, and the resulting values are used to calculate the amplitude. The final values of sliding distance and its maximum will be used throughout for evaluation.

Unfortunately, the sliding distance gives only qualitative assessment for a static problem and doesn't give the true creep. For generating actual creep data, one needs to include the rotation of the bearing components which would allow the stick-slip conditions, generated in the static case, to circulate throughout the bearing circumference. The accumulation of relative micro-movements of the ring over multiple rotations would give quantitative creep results.

4.2 Qualitative results

4.2.1 Sliding distance evaluation

The sliding distance quantities are evaluated as follows:

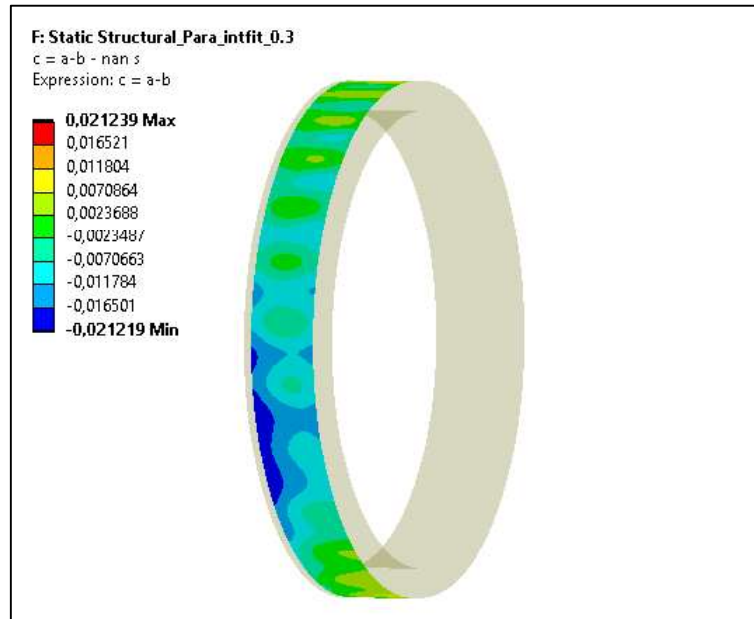


Figure 31: $TASR_0$

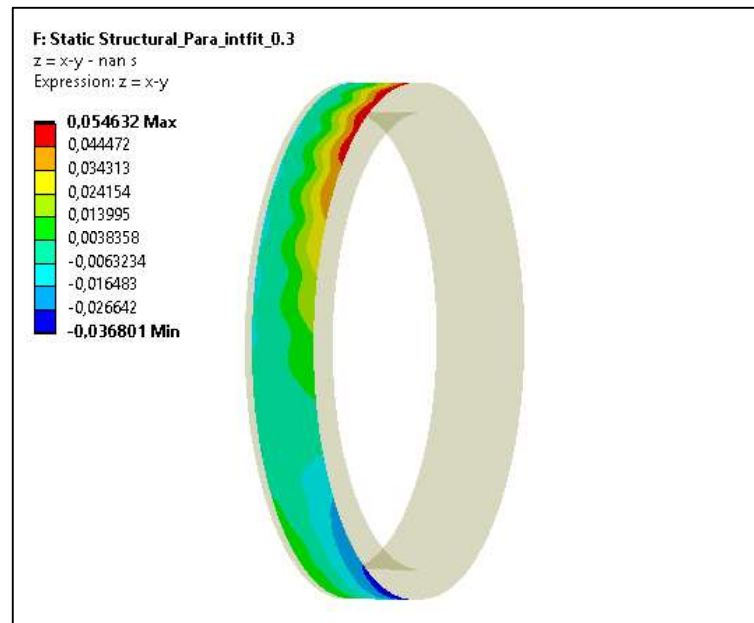


Figure 32: $TASS_0$

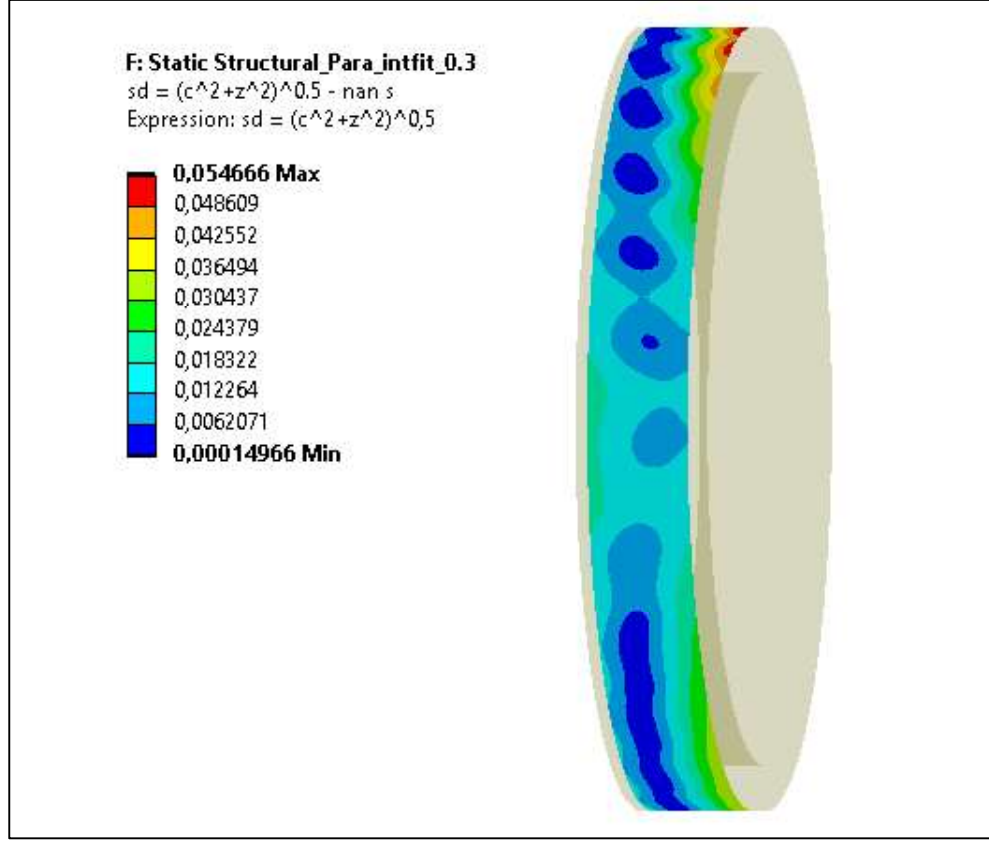


Figure 33: Sliding distance amplitude

As described in section 4.1, the TASS and TASR values are calculated for the load steps two and three. After following post-processing, we get the final sliding distance:

$$TASR_0 = TASR_{t=3} - TASR_{t=2}$$

$$TASS_0 = TASS_{t=3} - TASS_{t=2}$$

$$sd = \sqrt{(TASS_0)^2 + (TASR_0)^2}$$

In the result plot of calculated sliding distance (sd), we can clearly visualize the alternating roller effects caused due to wave-like deformation in the ring. Moreover, the bending of shaft is also influencing the sliding distance at the edges. Due to combination of both the effects, we can see high values of sliding near the sides of the ring and in some regions between rollers. The regions with high local sliding over the width of the ring will be more prone to creep.

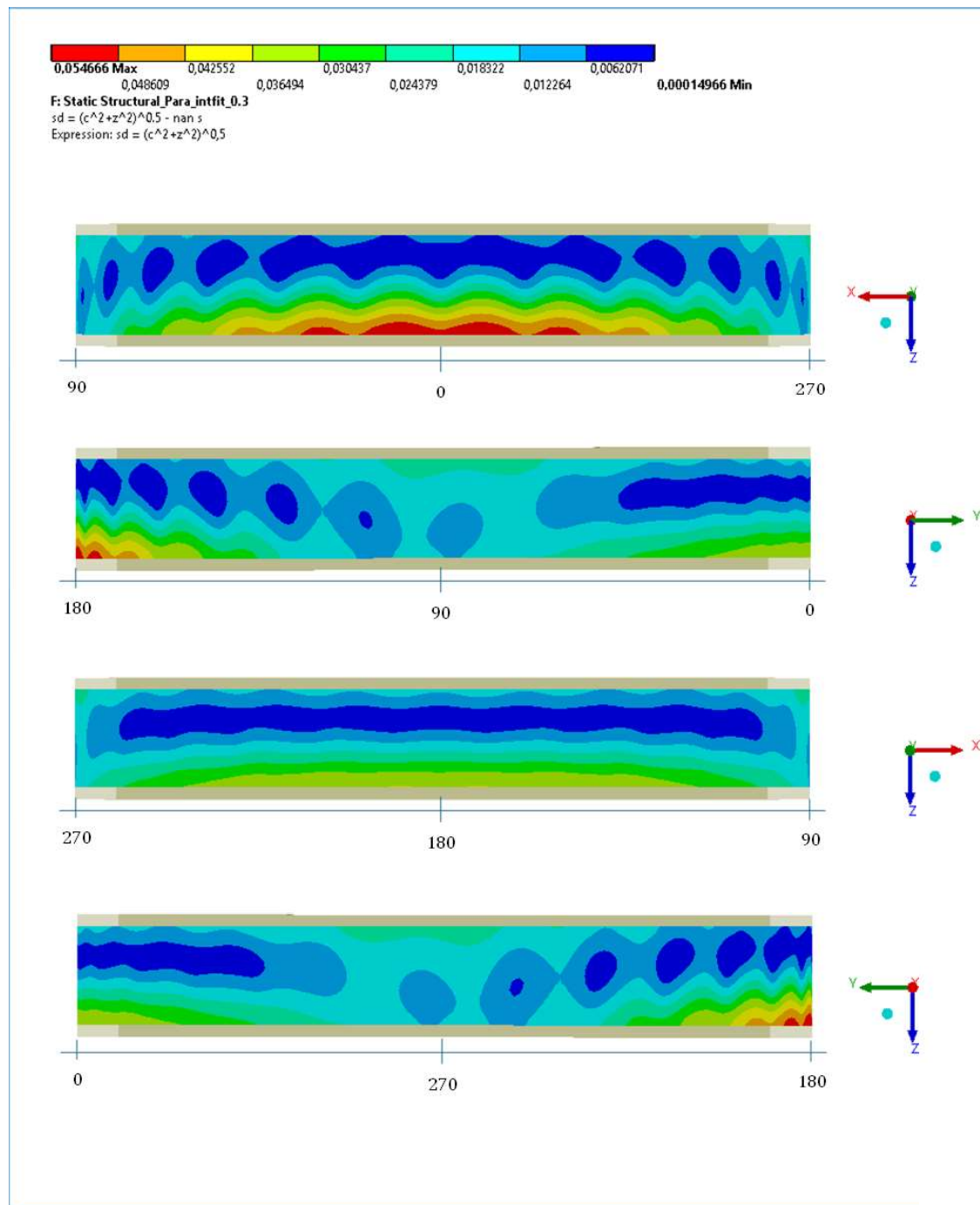


Figure 34: Calculated Sliding distance amplitude around the shaft

4.2.1 Contact status

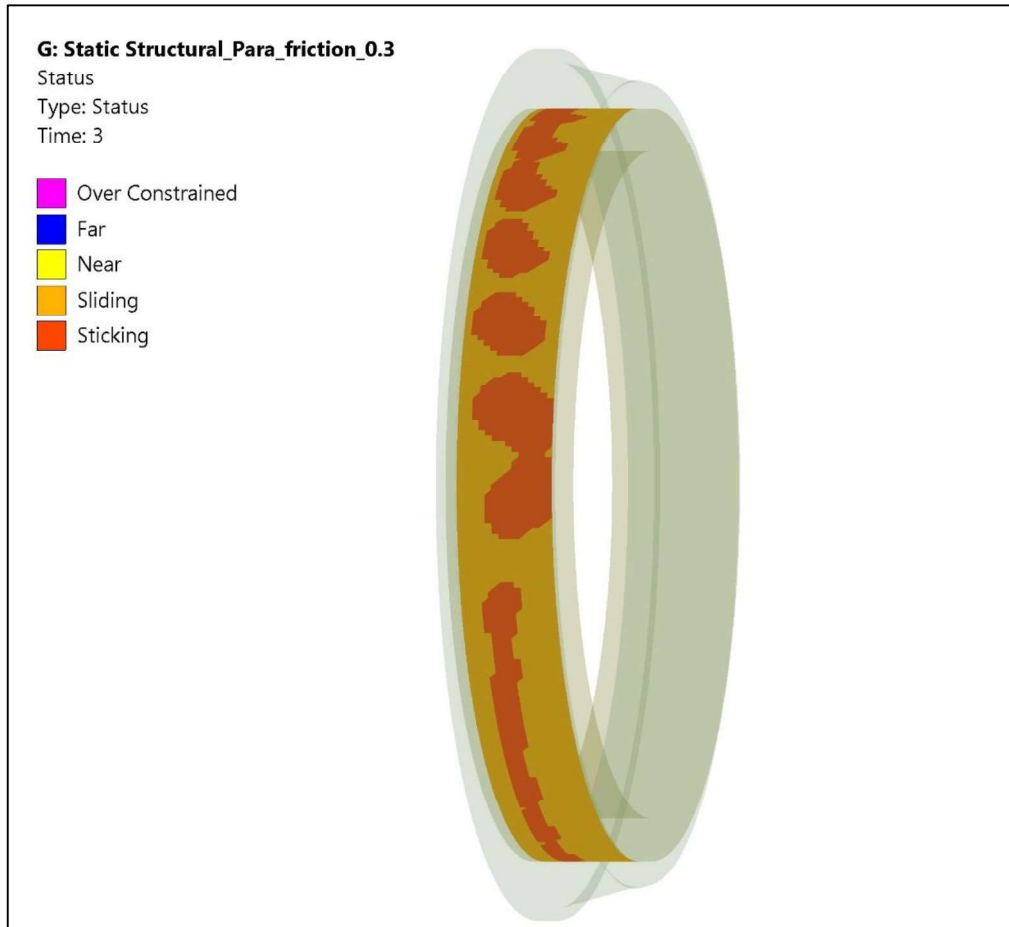


Figure 35: Contact status

The contact status plot generated for the model with certain input values of the influencing factors describes the stick-slip regions at the inner ring and shaft joint. The slip regions are dominant at both the edges of the ring and a pattern due to bending is also apparent. Most of these regions don't cover the entire width of the ring, but at some positions, the slip regions cover the entire or most of the width which could be of interest for further investigations of creep.

4.2.2 Parametric study 1

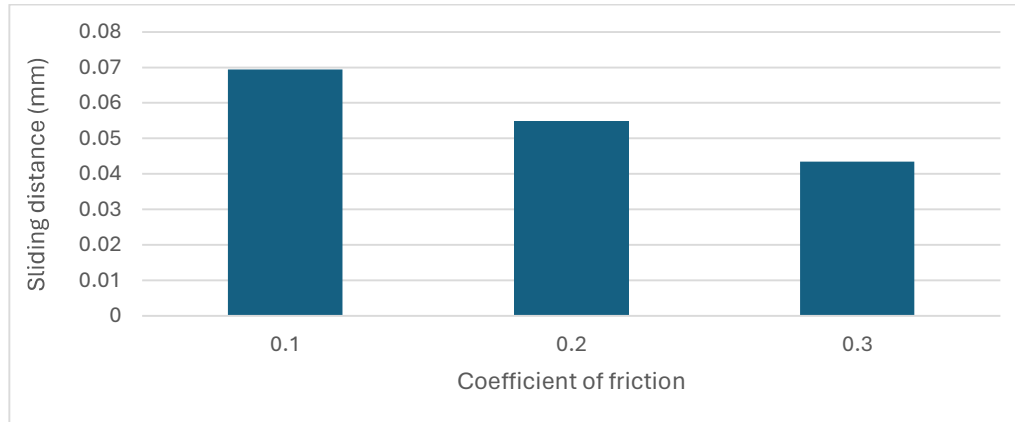


Figure36: Parametric study for coefficient of friction

	Coefficient of friction	max. Sliding distance (mm)
1	0.1	0.069476
2	0.2 ($\uparrow 100\%$)	0.054666 ($\downarrow 21\%$)
3	0.3 ($\uparrow 50\%$)	0.04349 ($\downarrow 20\%$)

In this parametric study the coefficient of friction is increased by 0.1 while keeping interference fit as 0.6mm and force as 10MN. As expected, we notice a drop in sliding distance values with the maximum value decreasing by around 20%. This shows that ring creep will decrease as well. Moreover, we know that the friction at the contact interface increases due to ‘run-in’ effect. Consequently, creeping tendency of ring will decrease over time when we consider the bearing in motion.

4.2.3 Parametric study 2

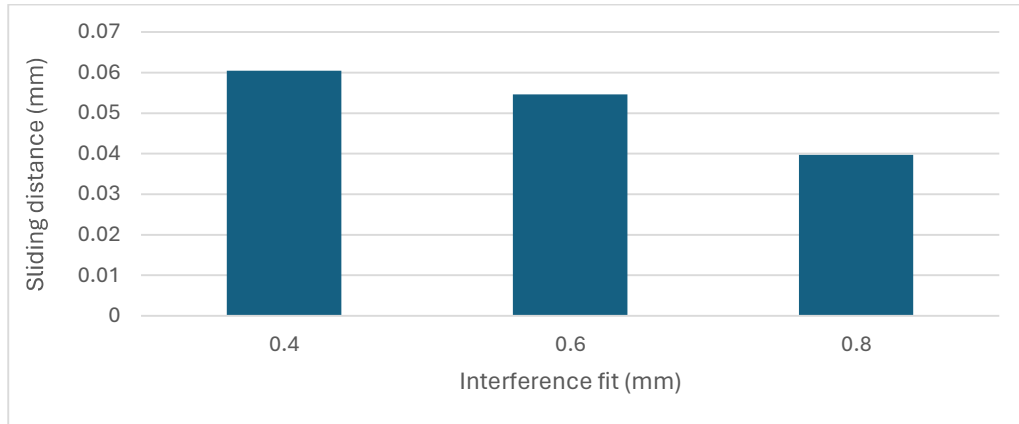


Figure 37: Parametric study for interference fit

	Interference fit (mm)	max. Sliding distance (mm)
1	0.4	0.060436
2	0.6 (\uparrow 50%)	0.054666 (\downarrow 10%)
3	0.8 (\uparrow 33%)	0.039756 (\downarrow 27%)

This is a parametric study on the overfit or interference fit between the main shaft and inner ring. The coefficient of friction has been set to 0.2 and force to 10 MN. One needs to be careful that the fit given is diametrical and must be halved for setting the offset value. From the values plotted it can be inferred that the sliding distance decreases by certain extent with increasing interference fit value. Correspondingly, the creeping tendency will tend to decrease as well. This is in accordance with the previous studies done on different kinds of bearings. Therefore, the overfit set during assembly must be large enough to avoid this phenomenon.

4.2.4 Parametric study 3

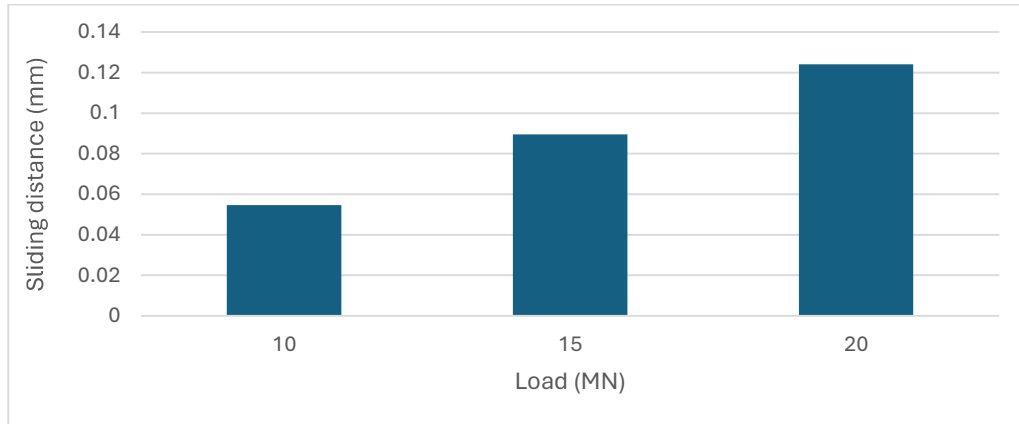


Figure 38: Parametric study for loading

	Load (MN)	max. Sliding distance (mm)
1	10	0.054666
2	15 (\uparrow 50%)	0.089608 (\uparrow 64%)
3	20 (\uparrow 33%)	0.1242 (\uparrow 39%)

The load at the flange end of the main shaft creates bending of that shaft and such deformation influences sliding distance significantly. Therefore, creeping tendency of the inner ring will increase if the load increases. Again, this influencing factor is consistent with the previous studies for different bearing types. The stresses caused by these increased forces could be well within the design limits. But this failure mode might still develop under such conditions and lead to damage or wear before the design-life.

4.3 Quantitative results

The creep is plotted quantitatively as tangential displacement over time. One of the nodes at the ring's inner surface is selected as a sensor. A node away from initial region of deformation can be chosen to start from a zero value.

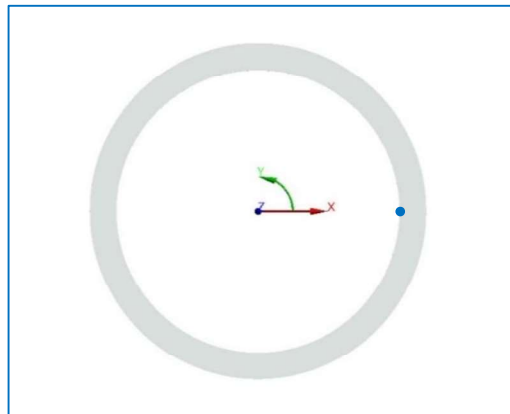


Figure 39: Node selected for evaluation

4.3.1 Creep plots

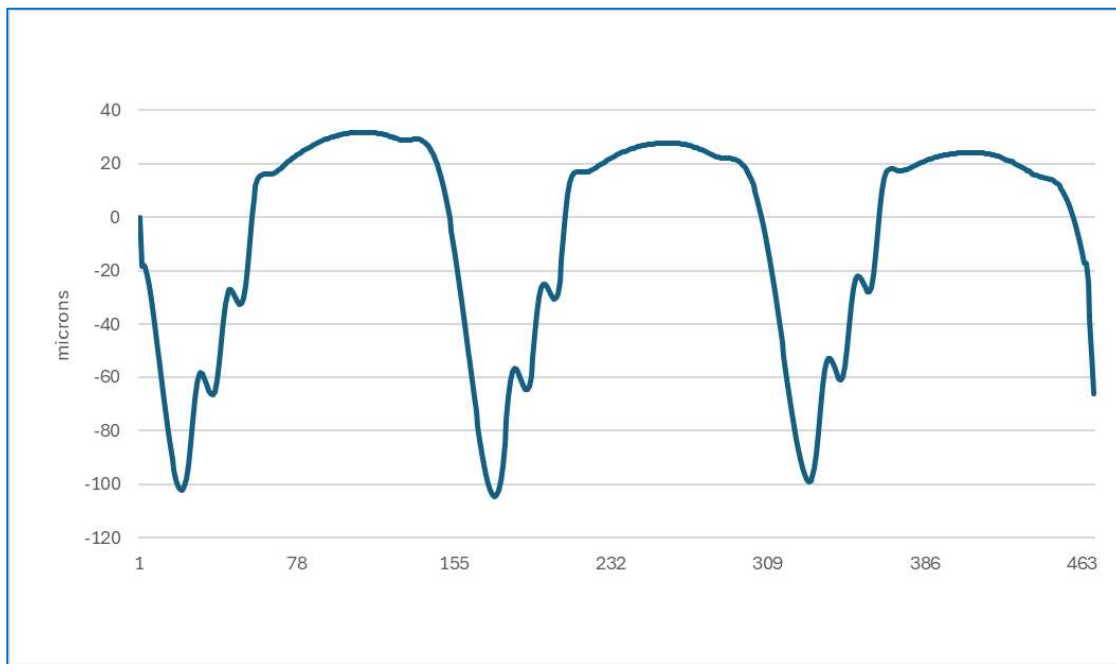


Figure 40: Tangential displacement (microns) over 3 rotations

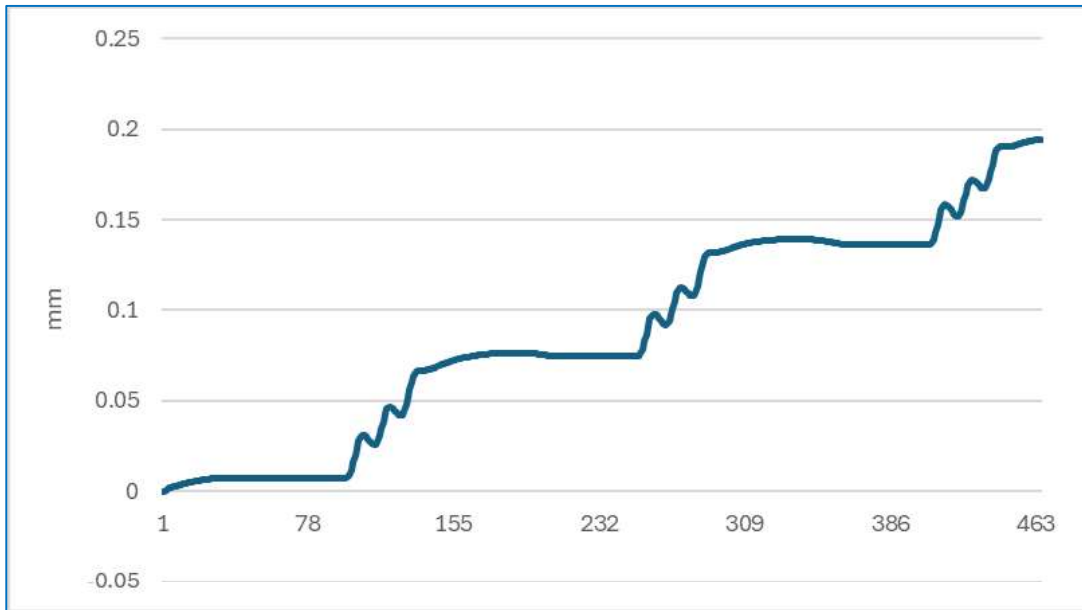


Figure 41: Sliding distance over 3 rotations

The tangential displacement is plotted for one of the nodes of the inner ring in contact with the shaft. The forces rotate 3 times along the inner ring surface. The time given on the horizontal axis need not be considered as per kinematics of the bearing, but to be used just for reference. A drift can be noticed in the plot over time which can be attributed to creep.

Moreover, the sliding distance can also be plotted for the same node over 3 rotations. We notice creeping behavior between the inner ring and shaft whenever the high contact forces (attributing to loaded roller elements) pass over this position.

4.3.2 Load vs tangential displacement (pattern and trend)

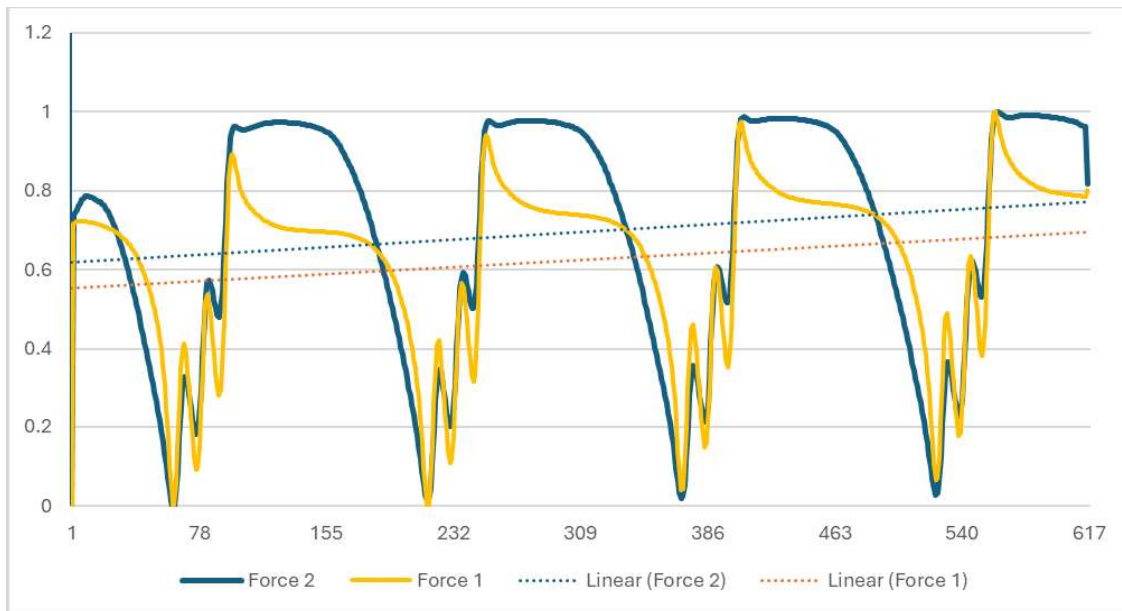


Figure 42: Normalised Tangential slip over 4 rotations for 2 different load cases.

The model is solved for a force 1MN (Force 1) and the contact forces rotated 4 times. The same model is solved for another force (Force 2) 10 times the previous one to check for the change in pattern of tangential displacement. The values of displacement change by the order of 10 as well and therefore they are normalized before plotting. Even though the pattern is different, the creeping behavior is similar, and both the plots show an increasing trend line.

5 Conclusion and Future work

The thesis investigated qualitative creep for the TRB which reduced rollers in the given drivetrain assembly and carried out 3 parametric studies. The sliding distance was evaluated for a given diametrical interference fit of 0.6mm and coefficient of friction of 0.2. The contact status exhibited the stick-slip regions over the inner ring and shaft frictional joint and conformed with the calculated sliding distance plot.

Further in the parametric studies, the sliding distance showed significant dependence on the interference fit and coefficient of friction. We could infer that the creep tends to decrease while increasing the values of both these parameters individually. Whereas the load highly influenced the sliding distance. It's evident that high loads increase the tendency to creep.

The behavior of these 3 parameters is in accordance with the previous studies on smaller bearing types [10] and it shows that the modeling approach for qualitative study is well suited for larger TRBs as well.

The approach developed for quantitative assessment of creep was for a smaller bearing due to requirement of high computational resources in case of the original TRB. The model was highly simplified by replacing the contacts with contact forces and providing rotations via scripting. The model showed good convergence for the simple friction model and the results of tangential slip and sliding distance exhibited a drift due to creeping behavior. But the values could only be validated via experimental setup. The sliding distance plot showed similar trends as compared with previous studies, but the quantitative values differ owing to complicated contact settings and formulations [10]. Therefore, this approach can be replicated for the bigger TRB in the given drivetrain assembly, but with some simplifications.

The contact parameters need to be investigated for this type of bearing by experiments and tests. Also, a friction model involving the run-in effect would give more realistic quantitative values for creep.

There are many more influencing factors which could be analyzed for sensitivity such as the housing stiffness, yaw and pitch movements of the turbine, roller slip, etc. Lastly, the model does not incorporate the kinematics of the roller elements. The distribution of contact forces varies after every degree of rotation, which could affect the creeping behavior. This could be scripted in APDL to account for the kinematics of the roller elements.

References

- [1] E. Hart and Clarke, "A review of wind turbine main bearings: design, operation, modelling, damage mechanisms and fault detection," *Wind Energy Science*, vol. 5, no. 1, pp. 105-124, 2020.
- [2] E. Hart and Turnbull, "Wind turbine main-bearing loading and wind field characteristics," *Wind Energy*, vol. 22, no. 11, pp. 1534-1547, 2019.
- [3] T. Rauert and J. Herrmann, "Fretting fatigue induced surface cracks under shrink fitted main bearings in wind turbine rotor shafts," *Procedia Structural Integrity*, vol. 2, pp. 3601-3609, 2016.
- [4] J. Kirsch and H. Kyling, "Optimized cast components in the drive train of wind turbines and inner ring creep in the main bearing seat," *Forschung im Ingenieurwesen*, vol. 85, no. 2, pp. 199-210, 2021.
- [5] Billenstein, Daniel and Neidnicht, "Simulative and Experimental Investigation of the Ring Creeping Damage Mechanism Considering the Training Effect in Large-Sized Bearings," *machines*, vol. 11, 2023.
- [6] A. Maiwald and E. Leidich, "FE simulations of irreversible relative movements (creeping) in rolling bearing seats--influential parameters and remedies," *World Congress on Engineering and Computer Science*, vol. 2, 2013.
- [7] F. Schlüter, Ring Creep in Wind Turbine Planetary Bearings, Doctoral dissertation, Fakultät für Maschinenwesen RWTH Aachen, 2022.
- [8] T. Niwa, "A creep mechanism of rolling bearings," *NTN Tech. Review*, vol. 81, pp. 100-103, 2013.
- [9] J. Murata and T. Onizuka, "Generation Mechanism of Inner Ring Creep," *Koyo Eng J*, vol. 166, pp. 41-47, 2005.
- [10] FVA-Nr. 479 III, Ringwandern bei angestellten Lagern und Radiallagern unter kombinierten Belastungen. FVA-Heft Nr. 1097, 2014.
- [11] FVA-Nr. 479 I, Wandernde Wälzlager Innen- und Außenringe unter verschiedenen Einsatzbedingungen, FVA-Heft Nr. 852, 2008.
- [12] Ansys Mechanical Theory Reference.
- [13] APDL Command Reference.

- [14] J. Zhan, K. Yukawa and H. Takemura , "Analysis of bearing outer ring creep with FEM," in *Advanced Tribology: Proceedings of CIST2008 & ITS-IFToMM2008*, Springer, 2010, pp. 237-238.
- [15] T. Nagatomo and D. G. Toth, "Investigation of the bearing damage progression starting from cone creep of a railroad axle journal bearing," *Quarterly Report of RTRI*, vol. 47, no. 3, pp. 119-124, 2006.
- [16] F. Harzendorf, R. Schelenz and G. Jacobs, "Method for holistic wind turbine drivetrain comparison exemplarily applied to geared and direct drive systems," *Forschung im Ingenieurwesen*, vol. 86, no. 1, pp. 21-33, 2022.

Appendix (A)

APDL script

```
9 ! Read csv file and store values in seperate arrays
10 to_skip = 1
11 /INQUIRE,numlines,LINEs,rollerforces3,csv
12 to_read = numlines - to_skip
13
14 *DEL, forces,,NOPR
15 *DIM, forces, TABLE,to_read-1,4
16 *TREAD, forces,rollerforces3,csv,,to_skip
17
18 *status, forces
19
20 *DEL, nodearray,,NOPR
21 *DIM, nodearray,ARRAY,to_read-1,1
22
23 *DEL, xforcearray,,NOPR
24 *DIM, xforcearray,ARRAY,to_read-1,1
25
26 *DEL, yforcearray,,NOPR
27 *DIM, yforcearray,ARRAY,to_read-1,1
28
29 *DEL, zforcearray,,NOPR
30 *DIM, zforcearray,ARRAY,to_read-1,1
31
32 *VFUN, nodearray(1),COPY,forces(1,1)
33 *VFUN, xforcearray(1),COPY,forces(1,2)
34 *VFUN, yforcearray(1),COPY,forces(1,3)
35 *VFUN, zforcearray(1),COPY,forces(1,4)
36
37 *DIM, xbuffarray,ARRAY,to_read-1,1
38 *DIM, ybuffarray,ARRAY,to_read-1,1
39 *DIM, zbuffarray,ARRAY,to_read-1,1
40
41 *status, nodearray
42 *status, xforcearray
43 *status, yforcearray
44 *status, zforcearray
45
46 !define offset and angle
47 !offset is the number of nodes along the width of the ring
48 !angle between two adjacent nodes
49
50 angle = 0.0408163265
51 offset = 17
52
53 ! Solve for n rotations
54 ! 1 rotation = number of divisions while defining mesh
55 ! n rotations = n*(no. of divisions)
```

```

56
57   SOLVE
58
59 * DO,T,2,614,1
60   TIME,T
61
62 * DO, Q, 1, to_read-1, 1
63   F, nodearray(Q), FX, 100*xforcearray(Q)
64   F, nodearray(Q), FY, 100*yforcearray(Q)
65   F, nodearray(Q), FZ, 100*zforcearray(Q)
66
67   xbuffarray(Q) = xforcearray(Q)*cos(angle)+yforcearray(Q)*sin(angle)
68   ybuffarray(Q) = yforcearray(Q)*cos(angle)-xforcearray(Q)*sin(angle)
69   zbuffarray(Q) = zforcearray(Q)
70
71   *ENDDO
72
73   !KBC,0
74   SOLVE
75
76 * DO, I, 1,to_read-offset-1,1
77   *VFUN, xforcearray(I), COPY, xbuffarray(I+offset)
78   *VFUN, yforcearray(I), COPY, ybuffarray(I+offset)
79   *VFUN, zforcearray(I), COPY, zbuffarray(I+offset)
80   *ENDDO
81
82 * DO, I, 1, offset,1
83   *VFUN, xforcearray(to_read-offset+I-1), COPY, xbuffarray(I)
84   *VFUN, yforcearray(to_read-offset+I-1), COPY, ybuffarray(I)
85   *VFUN, zforcearray(to_read-offset+I-1), COPY, zbuffarray(I)
86   *ENDDO
87
88   *ENDDO

```
